doi:10.1006/jmbi.2000.4082 available online at http://www.idealibrary.com on IDEAL® *J. Mol. Biol.* (2000) **302**, 671–689

JMB

High-resolution Solution Structure of the Catalytic Fragment of Human Collagenase-3 (MMP-13) Complexed with a Hydroxamic Acid Inhibitor

Franklin J. Moy[1], Pranab K. Chanda[2], James M. Chen[1], Scott Cosmi[2] Wade Edris[2], Jeremy I. Levin[3] and Robert Powers[1]*

[1]*Department of Biological Chemistry, Wyeth Research 85 Bolton St., Cambridge MA 02140, USA*

[2]*Department of Core Biotechnology, Wyeth Research CN, 8000, Princeton NJ 08543, USA*

[3]*Department of Chemical Sciences, Wyeth Research, 401 N. Middletown Rd. Pearl River, NY 10965, USA*

**Corresponding author*

The high-resolution solution structure of the catalytic fragment of human collagenase-3 (MMP-13) complexed with a sulfonamide derivative of a hydroxamic acid compound (WAY-151693) has been determined by multidimensional heteronuclear NMR. A total of 30 structures were calculated for residues 7-164 by means of hybrid distance geometry-simulated annealing using a total of 3280 experimental NMR restraints. The atomic rms distribution about the mean coordinate positions for the 30 structures is 0.43(±0.05) Å for the backbone atoms, 0.80(±0.09) Å for all atoms, and 0.47(±0.04) Å for all atoms excluding disordered side-chains. The overall structure of MMP-13 is composed of a β-sheet consisting of five β-strands in a mixed parallel and anti-parallel arrangement and three α-helices where its overall fold is consistent with previously solved MMP structures. A comparison of the NMR structure of MMP-13 with the published 1.6 Å resolution X-ray structure indicates that the major differences between the structures is associated with loop dynamics and crystal-packing interactions. The side-chains of some active-site residues for the NMR and X-ray structures of MMP-13 adopt distinct conformations. This is attributed to the presence of unique inhibitors in the two structures that encounter distinct interactions with MMP-13. The major structural difference observed between the MMP-13 and MMP-1 NMR structures is the relative size and shape of the S1′ pocket where this pocket is significantly longer for MMP-13, nearly reaching the surface of the protein. Additionally, MMP-1 and MMP-13 exhibit different dynamic properties for the active-site loop and the structural Zn-binding region. The inhibitor WAY-151693 is well defined in the MMP-13 active-site based on a total of 52 distance restraints. The binding motif of WAY-151693 in the MMP-13 complex is consistent with our previously reported MMP-1:CGS-27023A NMR structure and is similar to the MMP-13: RS-130830 X-ray structure.

Keywords: NMR; solution structure; matrix metalloproteinase; hydroxamic acid; human collagenase-3

Present addresses: J. M. Chen, Tularik Inc., Two Corporate Drive, South San Francisco, CA 94010, USA.

Abbreviations used: MMP-13, matrix metalloproteinase-13; HSQC, heteronuclear single-quantum coherence spectroscopy; HMQC, heteronuclear multiple-quantum coherence spectroscopy; TPPI, time-proportional phase incrementation; NOE, nuclear Overhauser effect; NOESY, nuclear Overhauser enhanced spectroscopy; TOCSY, total correlated spectroscopy; COSY, correlated spectroscopy; HNHA, amide proton to nitrogen to $C^{\alpha}H$ proton; HNHB, amide proton to nitrogen to $C^{\beta}H$ proton correlation; CT-HCACO, constant time $C^{\alpha}H$ proton to α-carbon to carbonyl correlation and HACAHB, $C^{\alpha}H$ proton to α-carbon to $C^{\beta}H$ proton correlation; SA, simulated annealing; THF, tetrahydrofuran; DMF, *N*,*N*-dimethylformamide; SAR, structure activity relationship.

E-mail address of the corresponding author: powersr@war.wyeth.com

0022-2836/00/030671–19 $35.00/0

Introduction

Human collagenase-3 (MMP-13) is a member of the matrix metalloproteinase (MMP) family, which includes the collagenases, stromelysins and gelatinases. The MMPs are involved in the degradation of the extracellular matrix, which is associated with normal tissue remodeling processes such as pregnancy, wound healing, and angiogenesis. The MMPs are a highly active set of targets for the design of therapeutic agents for the disease areas of arthritis and oncology (for reviews, see Browner, 1995; De *et al*., 1999; Morphy *et al*., 1995; Ries & Petrides, 1995; Woessner, 1991; Zask *et al*., 1996). MMP expression and activity is highly controlled because of the degradative nature of these enzymes. The apparent loss in this regulation results in the pathological destruction of connective tissue and the ensuing disease-state. MMP-13 was recently identified on the basis of differential expression in normal breast tissues and in breast carcinoma. In addition, its expression has been reported in squamous cell carcinomas of the larynx, head and neck, HCS-2/8 human chondrosarcoma cells, during fetal ossification and in articular cartilage of arthritic patients (Balbin *et al*., 1999).

There have been a number of X-ray and NMR structures solved for the catalytic domain of MMPs complexed with a variety of inhibitors (Becker *et al*., 1995; Betz *et al*., 1997; Bode *et al*., 1994; Botos *et al*., 1996; Broutin *et al*., 1996; Gonnella *et al*., 1995, 1997; Gooley *et al*., 1994, 1996; Lovejoy *et al*., 1994a,b,c; Moy *et al*., 1998, 1999; Spurlino *et al*., 1994; Stams *et al*., 1994; Van Doren *et al*., 1995) where the X-ray structure of MMP-13 was determined only recently (Lovejoy *et al*., 1999). There is a close similarity in the overall 3D fold for these proteins consistent with the relatively high level of sequence homology (>40 %). Despite this similarity in the MMP structures, there is distinct substrate specificity between these enzymes, indicative of specific biological roles for the various MMPs and a corresponding association with unique disease processes. One example of this potential specificity is the over-expression of MMP-13 in breast carcinoma and MMP-1 in papillary carcinomas. Therefore, the current paradigm in the development of MMP inhibitors is to design specificity into the structures of the small molecule instead of developing a broad-spectrum MMP inhibitor (Birkedal-Hansen *et al*., 1993; Rockwell *et al*., 1996). The rationale behind this approach is that an inhibitor specific for the MMP uniquely associated with a disease process may potentially minimize toxic side-effects (Drummond *et al*., 1999). Therefore, extensive structural information for the various MMPs is critical for a structure-based approach in designing inhibitor selectivity (Birkedal-Hansen *et al*., 1993; Ghose *et al*., 1995; Hajduk *et al*., 1997; Olejniczak *et al*., 1997; Rockwell *et al*., 1996). Toward this goal, we have previously presented the refinement of a high-resolution solution structure of inhibitor-free MMP-1 (Moy *et al*., 1998) and the solution structure of the MMP-1:CGS-27023A complex (Moy *et al*., 1999). Here, we present the determination of the high-resolution solution conformation of the catalytic fragment of human collagenase-3 (MMP-13, where Y104 in the X-ray structure corresponds to Y1 in the NMR structure) complexed with a sulfonamide derivative of a hydroxamic acid compound (WAY-151693). These results provide the foundation for such a structure-based drug development program for designing specific MMP inhibitors.

Results and Discussion

WAY-151693 resonance assignments and bound conformation

The primary structure of WAY-151693 along with the proton-naming convention is shown in Figure 1. The NMR assignments for WAY-151693 in the MMP-13 complex followed established protocols using 2D ^{12}C-filtering experiments (Gemmecker *et al*., 1992; Ikura & Bax, 1992; Petros *et al*., 1992), since the NMR sample was composed of ^{13}C/^{15}N-labeled MMP-13 and unlabeled WAY-151693. Thus, traditional 2D-NOESY, COSY and TOCSY spectra of WAY-151693 in the presence of MMP-13 yielded the straightforward assignments for WAY-151693 (listed in supplementary Table 1S along with the assignments for free WAY-151693; see Materials and Methods). The only notable difference in the assignments for free and bound WAY-151693 is the observation of two distinct resonances for 2HB1/2 in the complex. The missing resonance in the free WAY-151693 structure may simply be obscured by water. Also, the observation that the protons on the *p*-methoxyphenyl ring are degenerate suggests rapid ring flips when complexed to MMP-13. This was seen with CGS-27023A complexed with both MMP-1 and stromelysin (Gonnella *et al*., 1997; Moy *et al*., 1999).

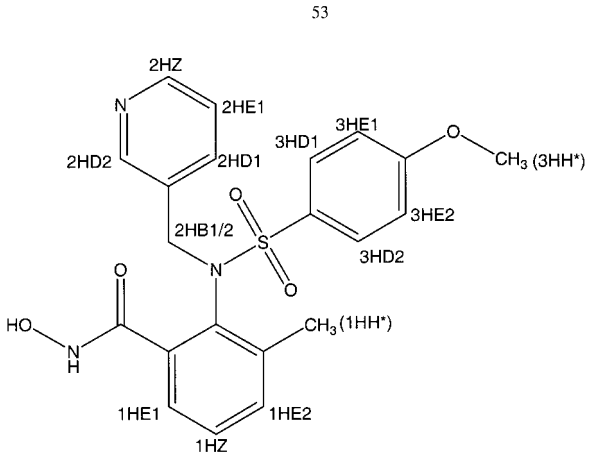

Figure 1. Illustration of the sulfonamide derivative of the hydroxamic acid inhibitor (WAY-151693) with the corresponding proton labels.

WAY-151693 does not adopt a preferred conformation in the absence of MMP-13, as evident by the lack of structural NOEs. Only a minimal number of intramolecular NOEs were observed for WAY-151693 in the MMP-13 complex, which were relevant to the bound conformation of WAY-151693 (supplementary Table 2S). The minimal number of structural NOEs is a result of the WAY-151693 conformation, structure and chemical shift degeneracy. A number of the observed NOEs correspond to a sequential interaction, have no effect on the overall conformation of the inhibitor and were not used in the refinement of WAY-151693 or the complex. The structural intramolecular NOEs observed are primarily between 1HH* and the pyridine ring and between 2HB1/2 and both the *p*-methoxyphenyl and aryl ring. These NOEs are consistent with the ''splayed'' conformation previously observed for CGS-27023A bound to both MMP-1 and stromelysin. The bound conformation of WAY-151693 is predominantly determined from the intermolecular NOEs between WAY-151693 and MMP-13 (supplementary Table 3S). A stereoview of the MMP-13 bound conformation of WAY-151693 is shown in Figure 2, along with the MMP-1 bound conformation of CGS-27023A for comparison.

Structure determination

The NMR structure determination methodology is an iterative procedure where the current state of the structure is used to analyze the ambiguous NOE data. In essence, the structure is used as a

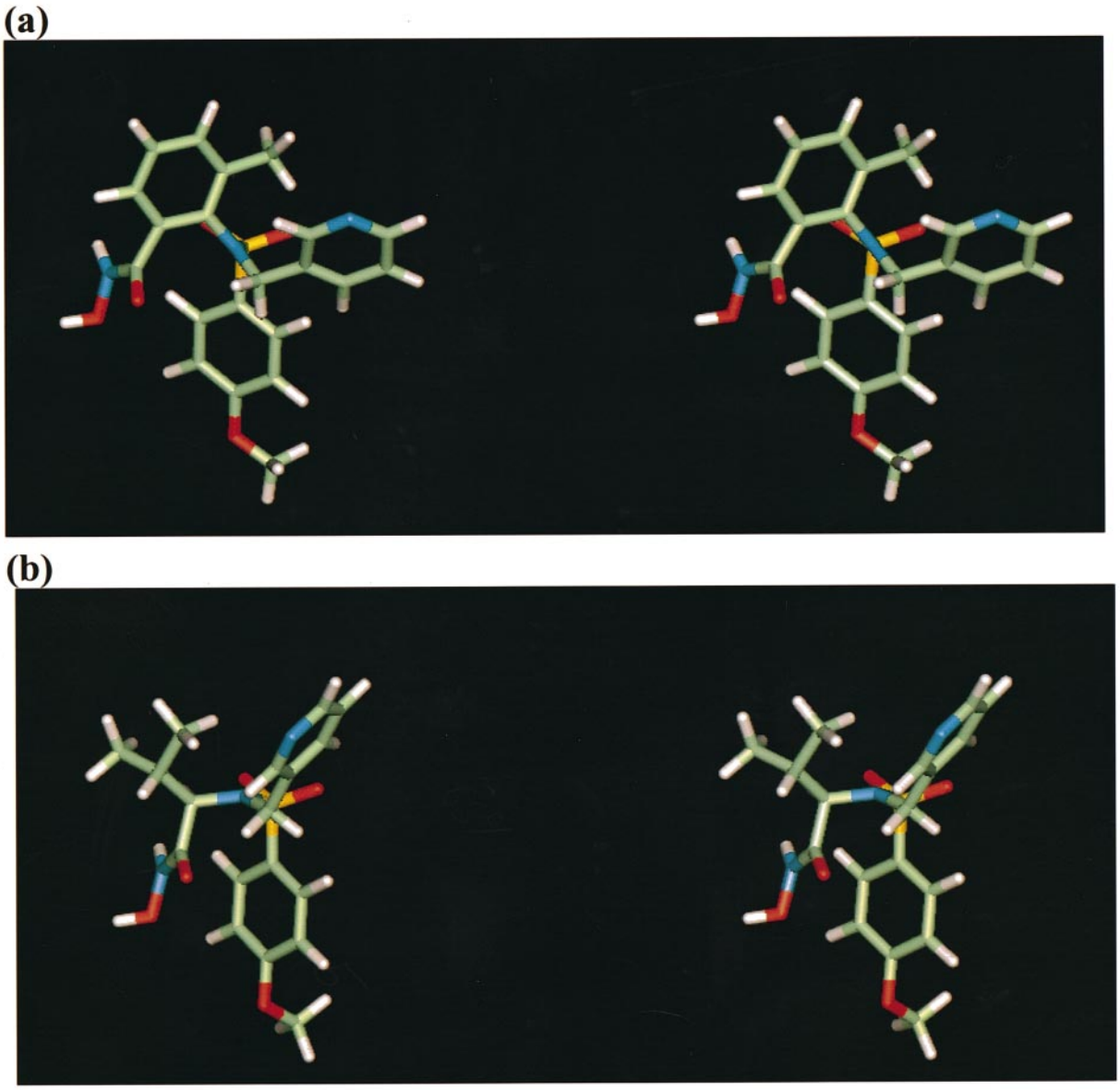

Figure 2. Cross-eyed stereoview of (a) the MMP-13 bound conformation of WAY-151693 and (b) the MMP-1 bound conformation of CGS-27023A.

distance filter to sort through the ambiguous NOE list where the first structure is determined from unambiguous data. For the refinement of MMP-13, the initial structure was a homology model based on the MMP-8 X-ray structure (Betz *et al*., 1997; Bode *et al*., 1994). This was justified by the overall similarity in previously reported MMP structures and from the secondary structure assignments by NMR for MMP-13. The regular secondary structure elements of MMP-13 were identified from a qualitative analysis of sequential and inter-strand NOEs, NH exchange rates, $^3J_{HN\alpha}$ coupling constants (Clore & Gronenborn, 1989) and the $^{13}C^{\alpha}$ and $^{13}C^{\beta}$ secondary chemical shifts (Spera & Bax, 1991). ^1H, ^{15}N, ^{13}C, and ^{13}CO assignments and initial secondary structure analysis of MMP-13 in the MMP-13:WAY-151693 complex have been reported (Moy *et al*., 2000). These data, together with the deduced secondary structure elements, are summarized in Figures 3 and 4. The deduced secondary structure is essentially identical with the previously reported inhibitor-free MMP-1 NMR structure (Moy *et al*., 1998).

The final 30 simulated annealing structures calculated for residues 7-164 were based on 3280 experimental NMR restraints, consisting of 2415 approximate interproton distance restraints, 47 distance restraints between MMP-13 and WAY-151693, five intramolecular distance restraints for WAY-151693, 88 distance restraints for 44 backbone hydrogen bonds, 391 torsion angle restraints, 103 $^3J_{NH\alpha}$ restraints 123 C^{α} restraints and 108 C^{β} restraints. Stereospecific assignments were obtained for 81 of the 100 residues with β-methylene protons, for the methyl groups of five of the six Val residues, and for the methyl groups of 12 of the 13 Leu residues. In addition, all 12 Phe residues and seven out of the eight Tyr residues were well defined, making it possible to assign NOE restraints to only one of the pair of $C^{\delta}H$ and $C^{\varepsilon}H$

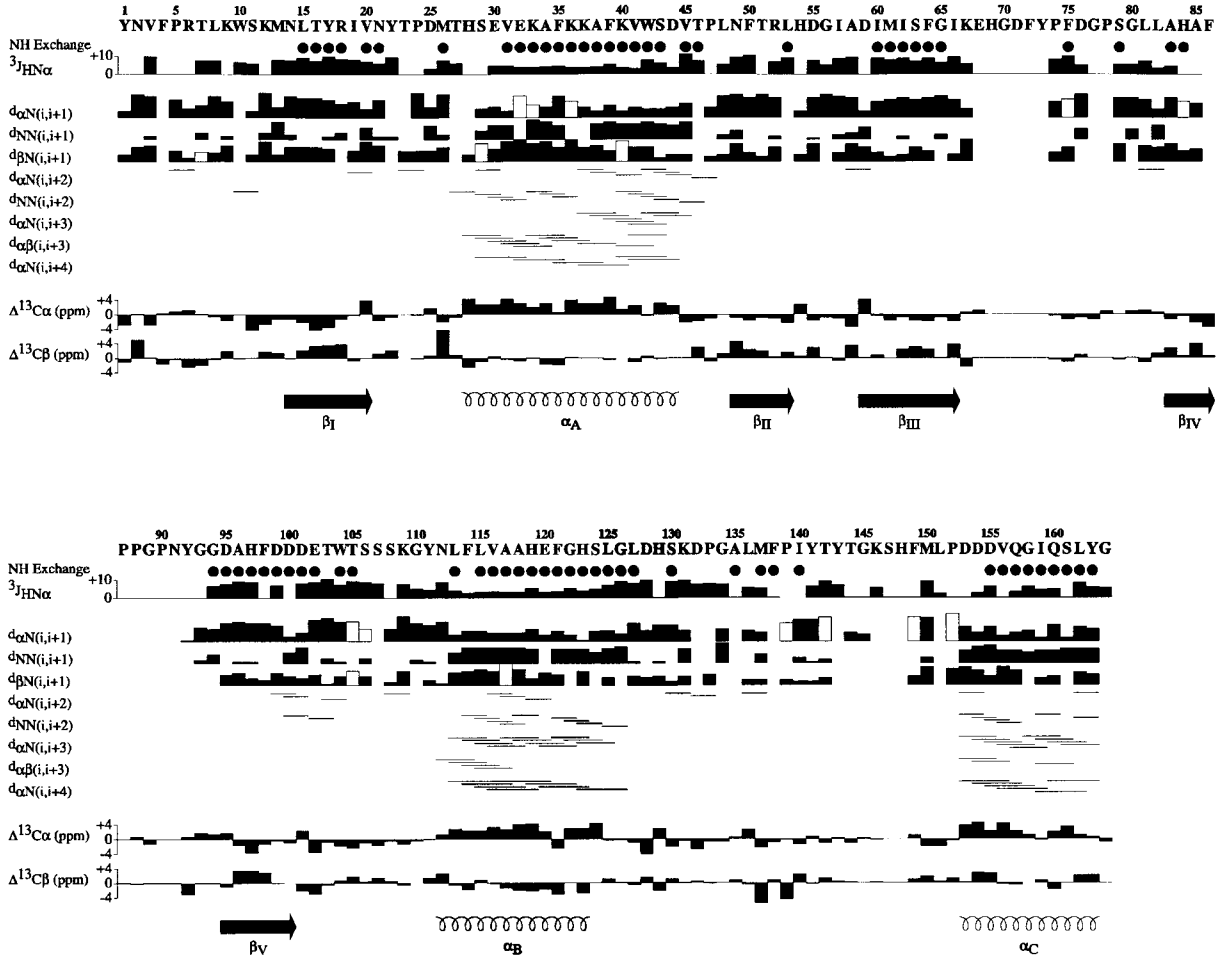

Figure 3. Summary of the sequential and medium-range NOEs involving the NH, H^{α} and H^{β} protons, the amide exchange and $^3J_{HN\alpha}$ coupling constant data, and the $^{13}C^{\alpha}$ and $^{13}C^{\beta}$ secondary chemical shifts observed for MMP-13 with the secondary structure deduced from these data. The thickness of the lines reflects the strength of the NOEs. Amide protons still present 24 hours after exchange to ^2H_2O are indicated by filled circles. The $^3J_{HN\alpha}$, $^{13}C^{\alpha}$ and $^{13}C^{\beta}$ secondary chemical shifts are shown as a bar graph. The open boxes represent potential sequential assignments NOEs that are obscured by resonance overlap and could therefore not be assigned unambiguously. The gray boxes on the same line as the $H^{\alpha}(i)$-NH$(i+1)$ NOEs represents the sequential NOE between the H^{α} proton of residue i and the $C^{\delta}H$ proton of the $i+1$ proline residue and is indicative of a *trans* proline.

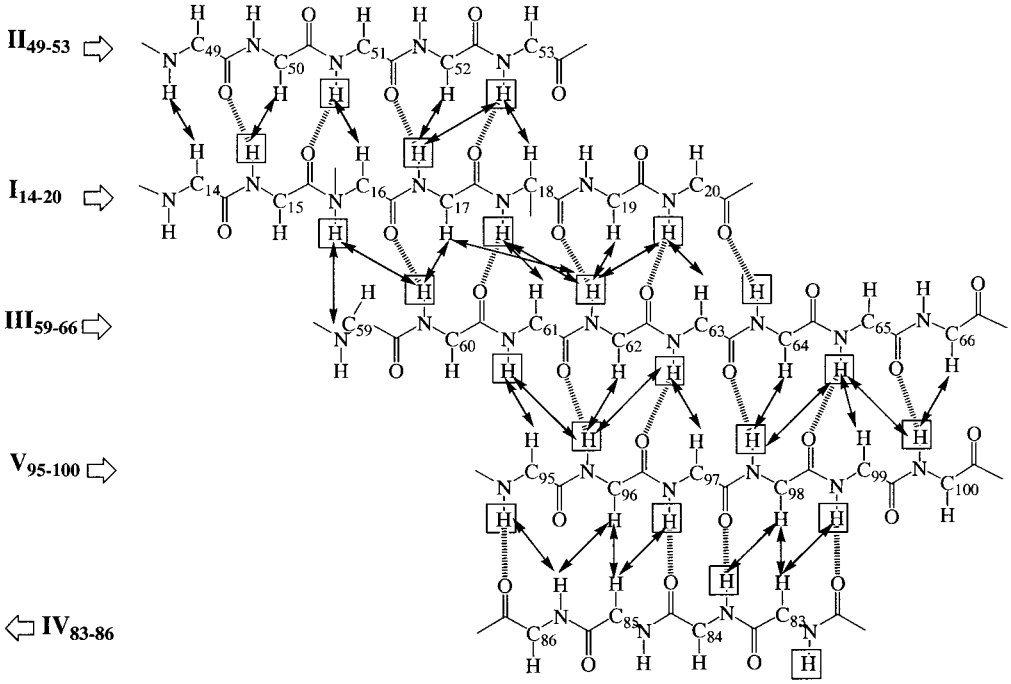

Figure 4. Secondary structure elements of MMP-13 as determined from qualitative analysis of the NOE and amide exchange data. The β-strands are indicated on the left by Roman numerals and the residue number range. Interstrand NOEs derived from the 3D ^{15}N and ^{13}C-edited NOESY spectra are indicated by arrows, and slowly exchanging amide protons are boxed. The hydrogen bonds deduced from these data are shown as broken lines.

protons and to assign a χ_2 torsion angle restraint. Similarly, χ_2 torsion angle restraints were assigned for the three Trp residues. A summary of the structural statistics for the final 30 simulated annealing (SA) structures of human MMP-13 is provided in Table 1, and a best-fit superposition of the backbone atoms and selected side-chains are shown in Figure 5. The atomic rms distribution of the 30 simulated annealing structures about the mean coordinate positions for residues 7-164 is 0.43(±0.05) Å for the backbone atoms, 0.80(±0.09) Å for all atoms, and 0.47(±0.04) Å for all atoms excluding disordered surface side-chains (Table 1). The mean standard deviation for the ϕ and ψ backbone torsion angles of residues 7-164 are 6.2(±11.3)° and 7.1(±11.8)°, respectively. The high quality of the MMP-13 NMR structure is also evident by the results of PROCHECK analysis and by a calculated, large negative value for the Lennard-Jones-van der Waals energy (−697(±12) kcal mol^{-1}). For the PROCHECK (Laskowski *et al.*, 1993) statistics, an overall *G*-factor of 0.16 ± 0.16, a hydrogen bond energy of 0.82 ± 0.05 and only 7.3 ± 0.9 bad contacts per 100 residues are consistent with a good-quality structure comparable to ~1 Å X-ray structure.

The high quality of the MMP-13 NMR structure is evident by the very small deviations from idealized covalent geometry, by the absence of interproton distance and torsion angle violations greater than 0.1 Å and 1°, respectively, and by the fact that most of the backbone torsion angles for non-glycine residues lie within expected regions of the Ramachandran plot: 92.2% of the residues lie within the most favored region of the Ramachandran ϕ,ψ plot and 7.8% in the additionally allowed regions. $^1J_{C\alpha H\alpha}$ coupling constants from the coupled CT-HCACO experiment indicated that all non-glycine residues have negative ϕ torsion angles (Vuister *et al.*, 1992).

The quality of the NMR data to properly define the complex is supported by the well-defined coordinates for WAY-151693 and the active-site residues, where the atomic rms distribution is 0.46(±0.10) Å and 0.18(±0.03) Å for the heavy atoms of WAY-151693 and MMP-13 backbone atoms, respectively.

Description of the MMP-13:WAY-151693 structure

The overall fold of MMP-13 is essentially identical with that of previously reported MMP structures (Becker *et al.*, 1995; Betz *et al.*, 1997; Bode *et al.*, 1994; Botos *et al.*, 1996; Broutin *et al.*, 1996; Gonnella *et al.*, 1995, 1997; Gooley *et al.*, 1994, 1996; Lovejoy *et al.*, 1994a,b,c; Moy *et al.*, 1998, 1999; Spurlino *et al.*, 1994; Stams *et al.*, 1994; Van Doren *et al.*, 1995). The MMP-13 NMR structure is composed of three α-helices corresponding to residues 28-44 (α_A), 112-123 (α_B) and 153-163 (α_C), and a mixed parallel and anti-parallel β-sheet consisting of five strands corresponding to residues 14-20 (β_I), 49-53 (β_{II}), 59-66 (β_{III}), 83-86 (β_{IV}) and 95-100 (β_V).

Table 1. Structural statistics and atomic rms differences

	⟨SA⟩	$(\overline{SA})_r$	X-ray[a]
A. *Structural statistics*			
rms deviations from experimental distance restraints (Å)[b]			
All (2555)	0.012 ± 0.002	0.009	0.262
Interresidue sequential ($\|i-j\|=1$) (643)	0.007 ± 0.004	0.005	0.121
Interresidue short range ($1<\|i-j\|\leqslant 5$) (480)	0.012 ± 0.003	0.008	0.296
Interresidue long-range ($\|i-j\|>5$) (749)	0.016 ± 0.002	0.013	0.390
Intraresidue (543)	0.007 ± 0.007	0.004	0.093
H-bonds (88)[c]	0.027 ± 0.002	0.019	0.147
Inhibitor (52)	0.003 ± 0.003	0.000	-
rms deviation from exptl dihedral restraints (deg.) (391)[b,d]	0.217 ± 0.108	0.212	30.2
rms deviation from exptl C^α restraints (ppm) (123)	0.98 ± 0.03	0.95	1.05
rms deviation from exptl C^β restraints (ppm) (108)	0.98 ± 0.02	0.97	0.97
rms deviation from $^3J_{NH\alpha}$ restraints (Hz) (103)	0.62 ± 0.02	0.66	1.31
E_{NOE} (kcal mol^{-1})[e]	20.3 ± 6.0	10.3	8497.8
E_{tor} (kcal mol^{-1})[e]	1.39 ± 1.63	1.08	21519
E_{repel} (kcal mol^{-1})[e]	44.9 ± 2.8	59.8	405.2
$E_{L\text{-}J}$ (kcal mol^{-1})[f]	−697 ± 12	−659	−964
Deviations from idealized covalent geometry			
Bonds (Å) (2525)	0.006 ± 0	0.003	0.092
Angles (deg) (4534)	0.507 ± 0.010	0.486	2.540
Impropers (deg.) (1385)[g]	0.363 ± 0.030	0.380	22.4
PROCHECK[i]			
Overall G-factor	0.16 ± 0.16	0.14	0.28
% Residues in most favorable region of Ramachandran plot	91.9 ± 1.2	92.2	90.6
H-bond energy	0.82 ± 0.05	0.80	0.80
Number of bad contacts/100 residues	7.3 ± 0.9	8.3	0

B. *Atomic rms differences (Å)*

		Active-site residues[i]		Residues 7-164		Secondary structure[j]		Ordered side-chain[k]
	WAY-151693[h]	Backbone	All	Backbone	All	Backbone	All	All
⟨SA⟩/$\overline{SA}$	0.46 ± 0.10	0.18 ± 0.03	0.31 ± 0.06	0.43 ± 0.05	0.80 ± 0.09	0.21 ± 0.03	0.53 ± 0.05	0.47 ± 0.04
⟨SA⟩/$(\overline{SA})_r$	0.51 ± 0.30	0.19 ± 0.04	0.34 ± 0.10	0.46 ± 0.06	0.90 ± 0.12	0.23 ± 0.03	0.61 ± 0.06	0.54 ± 0.05
$(\overline{SA})_r$/$\overline{SA}$	0.36	0.07	0.18	0.17	0.42	0.09	0.30	0.26
$\overline{SA}$/X-ray	-	0.85	1.34	1.30	1.72	0.94	1.42	1.45
$(\overline{SA})_r$/X-ray	-	0.87	1.38	1.31	1.77	0.96	1.47	1.48
⟨SA⟩/X-ray	-	0.87 ± 0.05	1.38 ± 0.05	1.37 ± 0.08	1.89 ± 0.07	0.95 ± 0.04	1.52 ± 0.04	1.53 ± 0.05

The structure refinement and corresponding constraints correspond only to residues 7-164 for MMP-13, residues 1-6 and 165 are highly disordered and were excluded from the structure calculations. The notation of the structures is as follows: ⟨SA⟩ are the final 30 simulated annealing structures; $\overline{SA}$ is the mean structure obtained by averaging the coordinates of the individual SA structures best fit to each other; and $(\overline{SA})_r$ is the restrained minimized mean structure obtained by restrained minimization of the mean structure $\overline{SA}$ (Nilges *et al*., 1988c). The number of terms for the various restraints is given in parentheses.

[a] X-ray is the 1.6 Å resolution X-ray structure from Lovejoy *et al*. (1999) (PDB 830C). Residues 145-149 are not present in the X-ray structure. Tyr and Phe χ_2 dihedral angles in the X-ray structure were changed to be consistent with the NMR structure, since it is not possible to differentiate between $+90^\circ$ or -90° in the X-ray structure. Without this correction, the calculation of E_{NOE} and E_{tor} would be artificially high for the X-ray structure.

[b] None of the structures exhibited distance violations greater than 0.2 Å or dihedral angle violations greater than 1°.

[c] For backbone NH-CO hydrogen bond there are two restraints: $r_{NH\text{-}O}$ = 1.5-2.3 Å and $r_{N\text{-}O}$ = 2.5-3.3 Å. All hydrogen bonds involve slowly exchanging NH protons.

[d] The torsion angle restraints comprise 134 ϕ, 116 ψ, 101 $\chi1$ and 40 $\chi2$ restraints.

[e] The values of the square-well NOE (E_{NOE}) and torsion angle (E_{tor}) potentials (cf. equations 2 and 3 of Clore *et al*., 1986) are calculated with force constants of 50 kcal mol^{-1} Å^{-2} and 200 kcal mol^{-1} rad^{-2}, respectively. The value of the quartic van der Waals repulsion term (E_{rep}) (cf. equation 5 of Nilges *et al*., 1988c) is calculated with a force constant of 4 kcal mol^{-1} Å^{-4} with the hard-sphere van der Waals radius set to 0.8 times the standard values used in the CHARMM (Brooks *et al*., 1983) emperical energy function (Nilges *et al*., 1988a,b,c).

[f] $E_{L\text{-}J}$ is the Lennard-Jones-van der Waals energy calculated with the CHARMM emperical energy function and is not included in the target function for simulated annealing or restrained minimization.

[g] The improper torsion restraints serve to maintain planarity and chirality.

[h] These values were calculated using the PROCHECK program (Laskowski *et al*., 1993). Only heavy atoms from the WAY-151693 structure were used for the rms calculation.

[i] The residues in the active-site correspond to 80-85, 112-124 and 134-143.

[j] The residues in the regular secondary structure are: 14-20(β_I), 49-53(β_{II}), 59-66(β_{III}), 83-86(β_{IV}), 95-100(β_V), 28-44(α_A), 112-123(α_B) and 153-163(α_C).

[k] The disordered side-chains that were excluded are as follows: inhibitor; residues 1-6; residues 165; Lys9 from C^δ; Lys12 from C^δ; Arg18 from C^γ; Tyr22 beyond C^δ; His28 from C^β; Glu30 from C^β; Glu32 from C^β; Lys33 beyond C^γ; Lys36 from C^γ; Lys37 from C^δ; Lys40 from C^δ; Arg52 from C^γ; His54 from C^β; Lys67 from C^β; Glu68 from C^β; His69 from C^β; Asp71 from C^β; Phe72 from C^β; Tyr73 from C^β; Pro74 from C^β; His84 from C^β; Pro90 from C^β; Asn91 from C^β; Tyr92 beyond C^β; Glu102 beyond C^β; Lys109 from C^δ; Glu120 beyond C^β; Lys131 from C^β; Lys146 from C^β; His148 from C^β; Met150 from C^β; Gln157 beyond C^β; Gln160 from C^β.

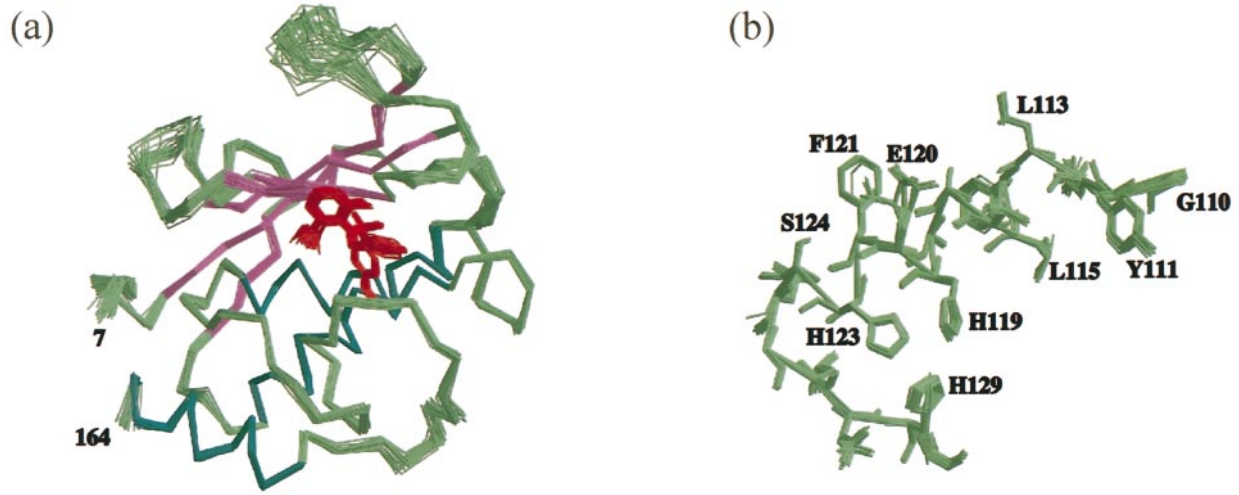

Figure 5. (a) The best-fit superposition of the backbone (N, C^{α}, C) for residues 7-164 and WAY-151693 heavy atoms (N, C, O, S) of the 30 final simulated annealing structures of MMP-13 complexed with WAY-151693. MMP-13 is colored by secondary structure and WAY-151693 is colored red. (b) All atoms of the 30 final simulated annealing structures for residues 110-130.

The active-site of MMP-13 is bordered by β-strand IV, the Ca^{2+}-binding loop, helix B and a random coil region from residues A135-T144. The catalytic zinc ion is chelated by H119, H123, and H129, while the structural zinc ion is chelated by H69, H84, and H97. The calcium ion is chelated in a loop region consisting of residues D75-G79. An interesting feature of the MMP active-site structure is an apparent kink in the backbone that occurs between the Ca^{2+}-binding loop and β-strand IV. In the case of MMP-13, this results in the NH groups of both L82 and A83 facing toward the active-site of the enzyme. An important feature of substrate and inhibitor binding to the MMPs are hydrogen bonding interactions with β-strand IV, which is facilitated by this unusual kink conformation (Borkakoti *et al*., 1994; Lovejoy *et al*., 1994b,c; Spurlino *et al*., 1994). A ribbon diagram of the restrained minimized average structure of the MMP-13:WAY-151693 is depicted in Figure 6(a).

The interaction of WAY-151693 in the active-site of MMP-13 was determined by five intramolecular NOEs for WAY-151693 and by a total of 47 intermolecular distance restraints between MMP-13 and WAY-151693 (supplementary Tables 2S and 3S). The key MMP-13 residues involved in the interaction with the inhibitor correspond to three distinct MMP-13 regions: residues L81, L82 and A83 from β-strand IV; residues L115, V116, and H119 from α-helix B; and L136, I140 and Y141 from the active-site loop, which comprise the S1′ and S2′ pockets of MMP-13. WAY-151693 binds to the right-hand side of the catalytic Zn ion where the *p*-methoxyphenyl group of WAY-151693 sits in the S1′ pocket of the MMP-13 active-site. This positioning is evident from the observed NOEs from 3HH*, 3HE1/2 and 3HD1/2 to L115, V116, H119, L136, and Y141. The aryl group primarily interacts with the side-chain of L81, as evident by the strong NOEs between 1HH*, 1HE2 and 1HZ and the L81 spin-system. Finally, the pyridine ring is essentially solvent-exposed but interacts with the side-chain of I140. These interactions position WAY-151693 such that the hydroxamic acid moiety of WAY-151693 chelates to the ''right'' of the catalytic zinc and the sulfonyl oxygen atoms are in hydrogen-bonding distance from the backbone NH of L82 from β-strand IV. An expanded view of the fit of WAY-151693 in the S1′ and S2′ pockets of MMP-13 is shown in Figure 6(b).

A feature of the MMP-13 structure is the large S1′ pocket relative to that of other MMPs, such as MMP-1, MMP-8 and matrilysin (Figure 7) (Moy *et al*., 1999). The large S1′ pocket for MMP-13 viewed from the active-site Zn ion nearly reaches the surface of the protein. The size of the S1′ pocket for MMP-13 is comparable with that for MMP-3 (stomelysin) but differs in the overall shape of the pocket (Moy *et al*., 1999). The different MMP subtypes are distinguished, in part, by substrate specificity where the unique size and shape differences in the S1′ pocket may contribute to some of the observed substrate specificity. However, the hemopexin domain in the intact MMP structure has been shown to be important for both selectivity and activity against native substrates (Cawston, 1996; Netzel-Arnett *et al*., 1993; Powell & Matrisian, 1996; Woessner, 1991).

It is interesting to note that the active-site loop (P138-G144) is highly dynamic in both the inhibitor-free MMP-1 and MMP-1:CGS-27023A complex structures based on the generalized order-parameters (S^2) (Moy *et al*., 1997). This region in the MMP-13:WAY-151693 structure appears to be less mobile, in that most of the residues in this loop region were easily observable in the ^{1}H-^{15}N HSQC spectra and readily assigned. Additionally, the generalized order-parameters (S^2) determined for the MMP-13:WAY-151693 structure have increased (Figure 8) relative to MMP-1, consistent with a

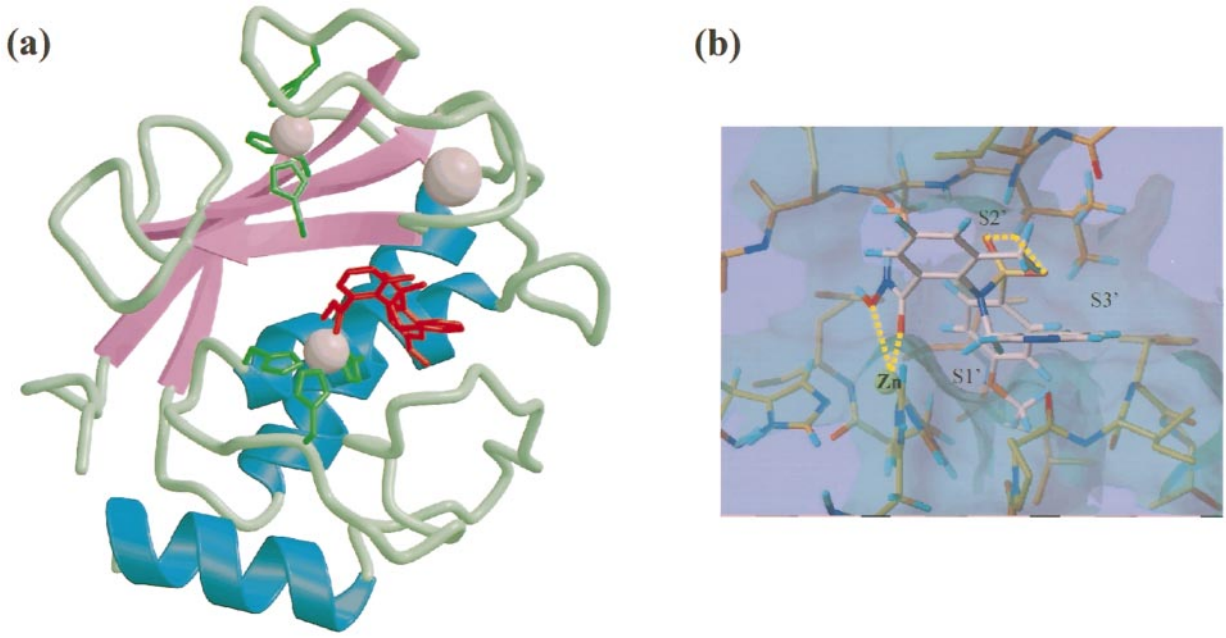

Figure 6. (a) Ribbon drawing of the restrained minimized mean structure of the MMP-13:WAY-151693 complex. MMP-13 is colored by secondary structure consistent with Figure 5(a) where the calcium and zinc ions are shown as van der Waal spheres. The inhibitor (red) and histidine side-chains (green) that chelate the zinc ions are shown as liquorice bonds. (b) Expanded view of the MMP-13:WAY-151693 complex where the MMP-13 active-site is shown as a Connolly surface with WAY-151693 shown as liquorice bonds. The view is looking down the S1′ pocket.

decrease in mobility for the active-site loop in MMP-13. It is important to note that while the active-site loop in MMP-13 demonstrates an increase in S^2 values relative to MMP-1, most of these residues exhibit S^2 values (0.67-0.78) lower then the average value (0.88 ± 0.07) for the structure. This implies that the active-site loop maintains some mobility relative to the remainder of the MMP-13 structure. One possible explanation for the difference in the mobility for the active-site loop between MMP-1 and MMP-13 is the hydrophobic interaction between the pyridine ring of WAY-151693 and the side-chain for I140. In MMP-1, I140 is replaced by a serine residue that essentially eliminates this beneficial interaction.

Another unique feature of the MMP-13 NMR structure is the apparent dynamic nature of residues H69 to Y73. These residues are completely disordered according to the lack of any assignment information, and the resulting absence of any constraint information is presumably a result of the flexible nature of these residues. Residues H69 to Y73 occur between the Ca^{2+}-binding loop and the structural zinc ion where the corresponding region in the previously solved MMP-1 NMR structures is well defined. There is no apparent explanation for this change in mobility between the two NMR structures but it may contribute to the observed difference in the physical behavior for MMP-1 and MMP-13. Under identical conditions, inhibitor-free MMP-1 is stable for upwards of two months whereas inhibitor-free MMP-13 effectively degrades rapidly at room temperature.

Comparison of the solution structure of MMP-13 with the X-ray structure

X-ray structures of MMP-13 complexed to diphenyl-ether sulphone-based hydroxamic acid inhibitors (RS-130830 and RS-113456) have been determined (Lovejoy *et al*., 1999). The superposition of the backbone atoms of the restrained minimized, $(SA)_r$, NMR structure of MMP-13 with the 1.6 Å X-ray structure (PDB 830C) is shown in Figure 9(a) with a plot of the backbone rms difference as a function of residue number (Figure 9(b)). Clearly, the overall folds of the two structures are similar, but distinct differences exist between the two structures, particularly in the loop regions, as evident by the rms difference between the two structures. For residues 7-164, the atomic rms difference between the minimized mean NMR structure, (SA)r, and the X-ray structure is 1.30 Å for the backbone atoms and 1.72 Å for all atoms (Table 1). When only residues involved in secondary structure regions are considered, these values drop to 0.94 Å and 1.42 Å, respectively. The comparison of the two structures improves slightly to 0.85 Å for the backbone atoms and 1.34 Å for all atoms when only residues in the active-site are compared. The majority of the differences between the NMR and X-ray structures appear to be associated with loop dynamics and crystal-packing interaction where the largest difference occurs in the loop region containing the structural Zn-binding site (residues 66-75) which is ''pushed-up'' relative to the MMP-13 X-ray structure. Residues H69 to

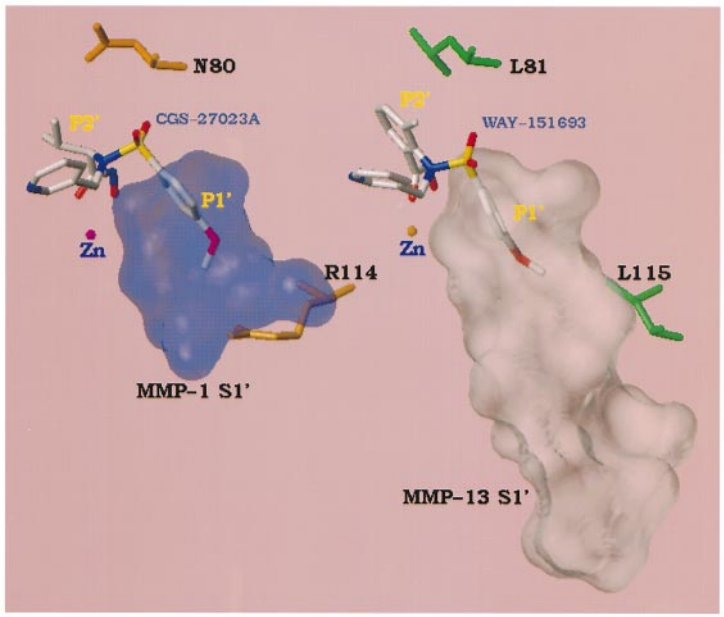


```
          77  *
MMP-1   GPgGnL AHA
MMP-13  GPsGlL AHA

          109     *                          *
MMP-1   re YNLhrVAAHE lGHSLGLsHS tDiGALMYPs YTF
MMP-13  kg YNLflVAAHE fGHSLGLdHS kDpGALMFPi YTYt
```

Figure 7. A graphics view describing the (left) MMP-1 and (right) MMP-13 regions of interest relative to the bound inhibitors CGS-27023A and WAY-151693, respectively. The inhibitors, catalytic zinc, S1′ pockets of MMP-1 (blue) and MMP-13 (white) and the side-chains corresponding to the MMP-1:N80 (orange) → MMP-13:L81 (green), MMP-1:R114 (orange) → MMP-13:L114 (green) and MMP-1:S139 (orange) → MMP-13:I140 (green) differences are labeled. (b) Sequential alignment of the MMP-1 and MMP-13 residues corresponding to the active-site. MMP-13 residues with an observed NOE to WAY-151693 are underlined. The sequence numbering is relative to MMP-13.

Y73 correspond to a region in the MMP-13 protein where the resonance assignments are incomplete (Moy *et al.*, 2000). This is consistent with a flexible region of the protein where the chemical shift resonances may be significantly broadened due to chemical exchange. Not unexpectedly, this region of the MMP-13 NMR structure exhibits the largest structural spread in the ensemble of structures (Figure 5). Interestingly, this region was readily assigned and did not exhibit any increased flexibility in the MMP-1 structure (Moy *et al.*, 1997), which may suggest a unique difference in the dynamic properties between MMP-1 and MMP-13.

Another significant perturbation between the NMR and X-ray structure of MMP-13 occurs in the loop region between β-strands β_{IV} and β_V, and the C terminus of β_V. This difference probably arises from a crystal packing interaction in the MMP-13 X-ray structure that brings residues F72, Y73 and Y92 into close contact with the symmetric dimer in the unit cell. Also, the loop region between β-strands β_{IV} and β_V appears to exhibit a higher order of mobility relative to the rest of the MMP-13 structure, based on the structural spread in the NMR ensemble. This is consistent with the observation that a majority of the residues in this loop exhibit ^{15}N T_2 exchange line-broadening, implying an additional motion on the 170 ns to 2.25 ms time-scale relative to a majority of the residues in the structure. This implies that the differences in the NMR and X-ray structures may also be a result of the flexibility of this loop in addition to the crystal packing interaction. A second crystal packing interaction may contribute to differences in helix α_C and residues 126-131. In the MMP-13 X-ray structure, the N-terminal residues 1-8 form a partial β-sheet interaction with residues 4-6 and 126-131 from the symmetric dimer, which also positions these residues proximal to helix α_C.

In the MMP-13 X-ray structure, residues 145-148 are not defined, due to a lack of electron density that is probably a result of local mobility for these residues. Similarly, these residues appear to be flexible in the MMP-13 NMR structure, as evident by the larger structural spread in the ensemble of structures relative to the core of the protein. Additionally, the generalized order-parameters (S^2) in this region of the protein (0.67-0.78) are less then the average value (0.88 ± 0.07) observed for the structure.

The local differences between the NMR and X-ray structures are indicated by the very high values of the NOE and torsion angle restraint energies, and by the number of interproton distance and torsion angle violations greater than 2 Å and 60°, respectively, exhibited by the X-ray structure (Table 2). A significant number of the larger violations can be attributed to different χ rotamers. There are a total of 28 residues between the NMR and X-ray structures that have distinctly different

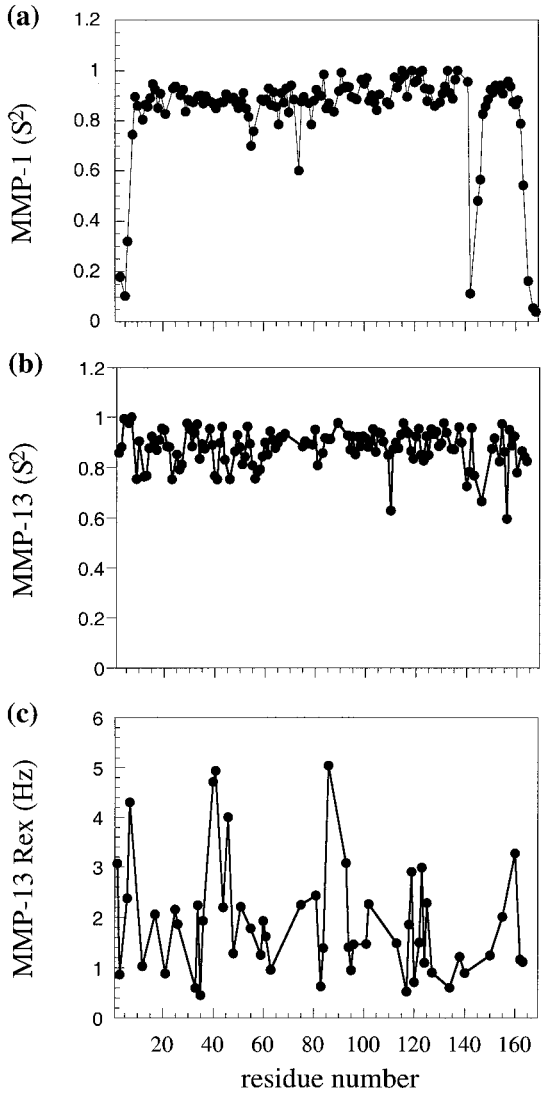

Figure 8. Generalized order-parameters (S^2) plotted on a per residue basis for (a) inhibitor-free MMP-1 (Moy *et al.*, 1997) and (b) the MMP-13:WAY-151693 complex. (c) ^{15}N T_2 exchange line-broadening (Rex) plotted on a per residue basis for the MMP-13:WAY-151693 complex.

χ rotamers. A vast majority of these residues are located in the crystal contact and flexibility regions previously discussed or are surface-exposed residues. The result is that the difference in the side-chain conformations has a minimal impact on the overall protein fold. Similarly, residues K67 and S79, which are located in the vicinity of the largest difference between the NMR and X-ray structure, exhibit a positive ϕ dihedral angle in the MMP-13 X-ray structure, which is not observed in the NMR structure. Nevertheless, the side-chain conformations of L81, L115, and L136 that are located in the enzyme active-site are distinctly different between the NMR and X-ray structure of MMP-13. These differences can be attributed directly to the distinct inhibitors present in the active-site for the NMR (WAY-151693) and X-ray structures (RS-130830) and the nature of the interaction with MMP-13 (Lovejoy *et al.*, 1999).

An expanded view of the MMP-13 active-site for the NMR and X-ray structure is presented in Figure 9(c). It is immediately apparent that, despite the chemical differences between the two inhibitors, the positioning of the two compounds in the active-site is very similar. Most notable is the overlap of the *p*-methoxyphenyl group from WAY-151693 with the biphenyl group from RS-130830. It is apparent that the unique features of the two inhibitors directly contribute to the differences in the conformation of L81, L115 and L136. The larger biphenyl group from RS-130830 reaches deeper into the S1′ pocket relative to WAY-151693. As a result, the side-chains of L115 and L136 move away from the inhibitor in the X-ray structure to accommodate RS-130830 in the S1′ pocket. An alternative view is that the side-chains of L115 and L136 move toward WAY-151693 in the NMR structure to improve the hydrophobic interaction with the *p*-methoxyphenyl group in the S1′ pocket. A similar effect causes the conformational change for L81. The pyran ring alpha to the hydroxamate group for RS-130830 is approximately perpendicular to β_{IV} compared to the parallel orientation of the aryl group from WAY-151693. Thus, the side-chain for L81 is required to move to optimize the interaction with either the pyran ring from RS-130830 or the aryl group from WAY-151693. It is evident from Figure 9(c) that the orientation of L81, L115 and L136 in the MMP-13:WAY-151693 complex would result in a steric clash with RS-130830. The comparison between the binding of MMP-13 with WAY-151693 and RS-130830 further supports the observation of a malleable MMP active-site (Lovejoy *et al.*, 1999; Moy *et al.*, 1997, 1998).

Comparison of the MMP-13:WAY-151693 and MMP-1:CGS-27023A structures

The high-resolution NMR structure for the MMP-13:WAY151693 complex was effectively and efficiently determined by using a homology model based on the MMP-8 X-ray structure as an initial structure to analyze ambiguous NOESY data (Betz *et al.*, 1997; Bode *et al.*, 1994). The use of the homology model for MMP-13 significantly expedited the process of determining the MMP-13 solution structure. This result is evidence of the high structural and sequence similarity between members of the MMP family and consistent with the previously observed best-fit superposition of the backbone atoms for MMP-1, stromelysin, matrilysin and neutrophil collagenase (Moy *et al.*, 1998, 1999).

The strong similarity between the various MMP structures creates an initial difficulty in designing specific MMP inhibitors. This is exemplified by the high level of sequence similarity among the MMPs in the active-site. Comparison of the sequence similarity between MMP-13 and MMP-1 illustrates this difficulty. There are only a few significant residue

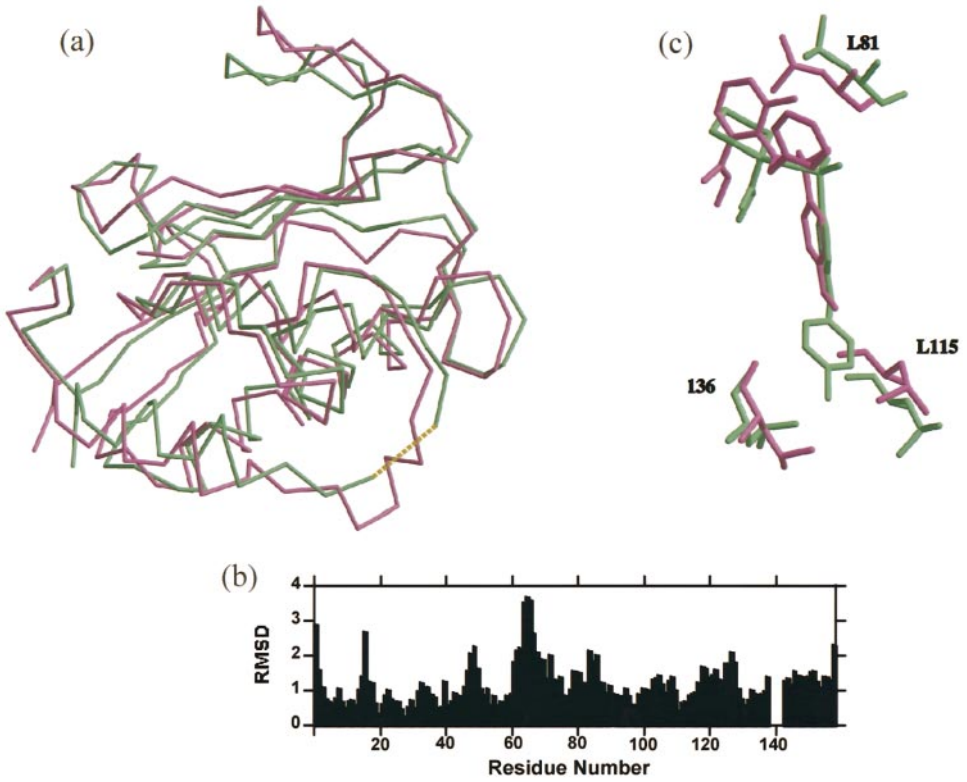

Figure 9. (a) Best fit superposition of the backbone (N, C^{α}, C) atoms of the restrained minimized mean NMR (blue) structure and the X-ray (green) structure of MMP-13 for residues 7-164. (b) Backbone (N, C^{α}, C, O) atomic rms differences between the restrained minimized mean NMR structure and the X-ray structure as a function of residue number. The X-ray structure is that by Lovejoy *et al*. (1999) (PDB 830C). (c) Expanded view of the active-site for the NMR (blue) and X-ray (green) structure of MMP-13 illustrating the overlap of WAY-151693 from the NMR structure with RS-130830 from the X-ray structure. The side-chains for L81, L115 and L136 that incur a conformational change in the presence of the two inhibitors are shown.

differences between the two enzymes where these modifications result in a significant change in the local environment of the active-site (Figure 7). The R114 to L115 modification results in a conversion from a hydrophilic to a hydrophobic residue at the base of the S1′ pocket between MMP-1 and MMP-13, respectively. The effect of the R114 to L115 substitution may be partially reduced, given the observation that R114 forms a hydrogen bond with a bound water molecule in the X-ray structure of MMP-1 (Spurlino *et al*., 1994). Conversely, there was no evidence in the NMR structure of inhibitor-free MMP-1 for the existence of any bound water in the active-site of the protein (Moy *et al*., 1998). Similarly, the N80 to L81 substitution places a bulkier hydrophobic residue in the S2′ pocket for MMP-13 compared to a more hydrophilic environment for MMP-1. Similarly in the active loop region, the bulky hydrophobic residue I140 in MMP-13 replaces the smaller hydrophilic S139 residue in MMP-1. Clearly, it is feasible to incorporate substituents into a small molecule to take advantage of these spatially distinct environmental changes between MMP-1 and MMP-13. Nevertheless, when these sequence and environmental differences are averaged across the MMP family it becomes less discriminating and extremely difficult to design an inhibitor to a specific MMP subtype based strictly on the small sequence differences.

Conversely, the most distinct structural difference between the MMPs and readily amenable to incorporating specificity in drug design is the relative size and shape of the S1′ pocket. This is clearly evident by comparison of the defined S1′ pockets for MMP-13 and MMP-1 depicted in Figure 7. The large difference in size in the S1′ pockets between the MMP-13 and MMP-1 NMR structures is striking. The large S1′ pocket for MMP-13 nearly reaches the outer surface of the protein as viewed from the active-site Zn ion and is greater then twice the size of the S1′ pocket for MMP-1. The additional size of the MMP-13 S1′ pocket relative to MMP-1 is best illustrated by the filling capacity of the two inhibitors. In the MMP-1:CGS-27023A NMR structure the *p*-methoxyphenyl group effectively fills the available S1′ pocket for MMP-1 (Moy *et al*., 1999). Conversely, in the MMP-13:WAY-151693 complex the *p*-methoxyphenyl group only partially fills the available space within the MMP-13 S1′ pocket (Figure 7). The size of the MMP-13 pocket is actually similar in size to that of stromelysin. The design of stromelysin inhibitors has taken advantage of this deeper S1′ pocket by using a biphenyl substituent in another series

Table 2. Number of violations exhibited by the X-ray structure of MMP-13 with respect to the experimental NMR interproton distance and torsion angle restraints

	0.1-0.3Å	0.3-0.5 Å	0.5-1.0 Å	1.0-2.0 Å	2.0-5.0 Å	>5.0 Å
A. *Number of violations in interproton distance restraints*						
All (2503)	42	26	38	34	11	0
Interresidue sequential ($\|i-j\|=1$) (643)	7	4	7	3	0	0
Interresidue short-range ($1<\|i-j\|\leqslant 5$) (480)	11	5	6	10	2	0
Interresidue long-range ($\|i-j\|>5$) (749)	15	12	20	19	9	0
Intraresidue (543)	6	4	3	2	0	0
H-bonds (88)	3	1	2	0	0	0
B. *Violations in torsion angle restraints*						
	10-30°	30-60°	60-120°	>120°		
All (391)	9	5	25	5		
ϕ (134)	3	1	1	0		
ψ (116)	3	1	1	0		
χ_1 (101)	3	1	20	1		
χ_2 (40)	0	2	3	4		

The X-ray structure of MMP-13 is the 1.6 Å resolution X-ray structure from Lovejoy *et al.* (1999) (PDB 830C). Residues 145-149 are not present in the X-ray structure. The total number of interproton distance and torsion angle restraints in each category is given in parentheses. Tyr and Phe χ_2 dihedral angles in the X-ray structure were changed to be consistent with the NMR structure, since it is not possible to differentiate between $+90°$ or $-90°$ in the X-ray structure. Without this correction, the number of violations would be artificially high for the X-ray structure.

instead of the *p*-methoxyphenyl group in WAY-151693 to bind into the S1′ pocket (Hajduk *et al.*, 1997; Olejniczak *et al.*, 1997). Thus, the NMR structures for MMP-13 and MMP-1 suggest that a ready approach to designing specificity between these MMPs is to take advantage of the significantly different sized S1′ pockets. In fact, this point was illustrated in the recently reported X-ray structure of MMP-13 (Lovejoy *et al.*, 1999). The high mobility of the MMP-1 active-site presents a potential caveat to this analysis of the static images of the MMP-1 and MMP-13 structures (Figure 8). It is probable that the MMP-1 active-site is capable of accommodating a S1′ substituent larger then implied from its current structure due to its increased mobility in both free and inhibited structures. The conformation of R114 has a significant impact on the overall size of the S1′ pocket for MMP-1. Recent X-ray structures of MMP-1 clearly indicate an inherent flexibility in R114, suggesting that the R114 side-chain may be displaced to optimize favorable interactions between MMP-1 and the inhibitor (Lovejoy *et al.*, 1999). The observed flexibility of the R114 side-chain in addition to the previous observation that residues P138-G144 in the active-site comprise a dynamic loop implies that the active-site of MMP-1 (Moy *et al.*, 1997), particularly the S1′ pocket, is not rigidly defined (Figure 8). The ''soft'' definition of the S1′ pocket also provides a potential explanation for the complicated SAR for MMP-1 inhibitors (Browner, 1995; De *et al.*, 1999; Morphy *et al.*, 1995; Ries & Petrides, 1995; Woessner, 1991; Zask *et al.*, 1996).

Examination of the binding mode of WAY-151693 in the MMP-13:WAY-151693 complex suggests a conformation generally similar to CGS-27023A in the MMP-1:CGS-27023A NMR structure previously reported (Figure 7) (Moy *et al.*, 1999). Nevertheless, the compounds exhibit different inhibitor activities relative to MMP-1 and MMP-13. The observed IC_{50} values for the two inhibitors with the two proteins are given in Table 3.

WAY-151693 and CGS-27023A are structurally very similar with the only difference being the nature of the substituent binding in the S2′ pocket. An aryl group in WAY-151693 replaces the isopropyl group in CGS-27023A. The strong resemblance between the binding mode of WAY-151693 and that of CGS-27023A is apparent from the nearly identical intermolecular NOE patterns observed between the inhibitors and the proteins. The key MMP-13 residues involved in the interaction with WAY-151693 correspond to L81, L82 and A83 from β-strand IV; residues L115, V116, and H119 from α-helix B; and L136, I140 and Y141 from the active-site loop. Similarly, the MMP-1 residues involved in the interaction with CGS-27023A correspond to residues N80, L81, A82 and H83 from β-strand IV; residues R114, V115, H118 and E119 from α-helix B; and L135, P138, Y137, S139 and Y140 from the dynamic flexible loop.

As stated previously, there are three distinct residue changes between MMP-13 and MMP-1 in the active-site. The R114 to L115 change between

Table 3. Inhibitor IC_{50}/K_i values (nM)

Inhibitor	MMP-13	MMP-1
WAY-151693	33	139
CGS-27023A	8	9
RS-130830	590	0.52

K_I values for RS-130830 as reported by Lovejoy *et al.* (1999).

MMP-1 and MMP-13, respectively, has a significant impact on the environment at the base of the S1′ pocket but since WAY-151693 only partially fills the MMP-13 S1′ pocket, this change should not effect the binding conformation of WAY-151693 relative to CGS-27023A. Conversely, the N80 to L81 substitution directly interacts with the inhibitors in the S2′ pocket and may result in an effective change in the binding mode of the inhibitors. To complicate the analysis, the only change in the inhibitors are the subsitutients that bind the S2′ pocket. For the MMP-1:CGS-27023A complex, the isopropyl group interacts with both the side-chains of N80 and H83 where the aryl group from WAY-151693 interacts only with L81 in MMP-13. While the conformation of N80 in MMP-1 has been shown to be dependent on the presence of an inhibitor, the conformation of H83 is primarily dependent on the interaction with the structural Zn ion (Moy *et al*., 1998, 1999). As a result, there is not a significant difference in the conformation of H83 between MMP-1 and MMP-13. Additionally, CGS-27023A is in hydrogen-bonding distance to both L81 and A82 where WAY-151693 appears to form a bifurcated hydrogen bond with L82 from β-strand IV. This analysis suggests that CGS-27023A binds closer to β-strand IV compared to WAY-151693, since the S2′ pocket is more accessible in MMP-1 due to the absence of the bulky L81 side-chain. The observed differences in the binding of CGS-27023A with MMP-1 and WAY-151693 with MMP-13 suggest a consistency with the observed differences in the IC_{50} values (Table 3).

The impact of the S139 to I140 residue difference between MMP-1 and MMP-13 on inhibitor binding appears to be related to a mobility change as opposed to a structural change. In the MMP-1:CGS-27023A structure, the pyridine ring position is essentially undefined and solvent-exposed (Moy *et al*., 1999). This compares to the MMP-13:WAY-151693 structure, where the pyridine ring interacts with the side-chain of I140. Clearly, Ile is a bulkier, more hydrophobic group relative to Ser, and provides a beneficial hydrophobic interaction with the pyridine ring of WAY-151693. The more interesting observation is the apparent decrease in mobility for the active loop in the MMP-13 structure that may be related to this interaction between the pyridine ring and I140. The decrease in mobility is suggested by the increase in the generalized order-parameters observed between the inhibitor-free MMP-1 and MMP-13:WAY-151693 structures (Figure 8). This decrease in mobility appears to be consistent with previous X-ray structures of inhibited MMPs (Spurlino *et al*., 1994) where the inhibitor may extend the formation of a β-sheet between β-strand IV and the active loop region resulting in low *B*-factors in the X-ray structure. Unlike the early peptide and peptide-mimics, the chemical nature of both CGS-27023A and WAY-151693 allow for the formation of hydrogen bonds only between the inhibitor and β-strand IV, but WAY-151693 does incur a positive interaction with the active loop that appears to decrease the mobility of the active loop region relative to the MMP-1:CGS-27023A structure. Therefore, the mobility of the active loop region may be easily removed through any positive interaction with an inhibitor.

While there are some interesting differences between the mode of binding for the two inhibitors in the MMP-13:WAY-151693 and MMP-1:CGS-27023A NMR structures, the more striking observation is the overall similarity between these two structures. Despite some significant sequence differences and a large difference in the size and shape of the S1′ pocket, either inhibitor structure would accurately predict the other structure. This observation seems to indicate that the major contributing factors to inhibitors binding the MMPs is the chelation of the hydroxamic acid to the catalytic zinc ion and the fit in the S1′ pocket. The interaction in the S2′ pocket appears to have a more subtle impact on inhibitor binding and selectivity, since both WAY-151693 and CGS-27023A are low nanomolar inhibitors of MMP-13 and MMP-1, respectively. Therefore, the high-resolution solution structure of the MMP-13:WAY-151693 in conjunction with the previously reported MMP-1 NMR structures suggest that taking advantage of the significant differences in the size and shape of the S1′ pocket is a reasonable approach for developing specific MMP inhibitors.

Materials and Methods

WAY-151693 synthesis

The sulfonamide derivative of the hydroxamic acid compound, WAY-151693, was prepared according to the following procedure. The sulfonamide derived from 2-amino-3-methyl-benzoic acid methyl ester and *p*-methoxybenzenesulfonyl chloride was alkylated with 3-picolyl chloride and the resulting ester was hydrolyzed (LiOH/THF) to afford the carboxylic acid. The hydroxamic acid was formed *via* the acid chloride (oxalyl chloride/DMF) followed by reaction with hydroxylamine. Conversion to the HCl salt yielded WAY-151693.

NMR sample preparation

The uniformly ^{15}N, ^{13}C-labeled 165 amino acid residue catalytic fragment of human collagenase-3 (MMP-13) was expressed in *Escherichia coli* strain BL21(DE3) containing the plasmid pProMMP-13 as described (Freije *et al*., 1994). MMP-13 was purified as described by Moy *et al*. (1997) with minor modifications. N-terminal amino acid sequencing was performed to confirm the protein's identity. The uniform ^{15}N and ^{13}C labeling of MMP-13 was confirmed by MALDI-TOF mass spectrometry (PerSeptive Biosystems) where label incorporation was $\geqslant 95\,\%$.

The MMP-13:WAY-151693 NMR sample contained 1 mM ^{15}N or $^{15}N/^{13}C$-labeled MMP-13 with WAY-151693 in a 1:1 ratio. The sample was prepared by repeated buffer exchange using 20-30 ml solution containing 10 mM deuterated Tris-base, 100 mM NaCl, 5 mM $CaCl_2$, 0.1 mM $ZnCl_2$, 2 mM NaN_3, 10 mM deut-

erated DTT, and 0.2 mM WAY-151693 in either 90% H_2O/10% ^2H_2O or 100% ^2H_2O. Buffer exchange was carried out on a Millipore Ultrafree-15 Centrifugal Filter Unit. Excess WAY-151693 was removed by additional buffer exchanges where WAY-151693 was removed from the buffer.

NMR data collection

All spectra were recorded at 35 °C on a Bruker AMX-2 600 spectrometer using a gradient-enhanced triple-resonance $^1H/^{13}C/^{15}N$ probe. For spectra recorded in H_2O, water suppression was achieved with the WATERGATE sequence and water-flip back pulses (Grzesiek & Bax, 1993; Piotto *et al.*, 1992). Quadrature detection in the indirectly detected dimensions were recorded with States-TPPI hypercomplex phase increment (Marion *et al.*, 1989b). Spectra were collected with appropriate refocusing delays to allow for 0,0 or −90,180 phase correction.

The resonance assignments and bound conformation of WAY-151693 in the MMP-13:WAY-151693 complex were based on the 2D $^{12}C/^{12}C$-filtered NOESY (Gemmecker *et al.*, 1992; Petros *et al.*, 1992), 2D $^{12}C/^{12}C$-filtered TOCSY (Gemmecker *et al.*, 1992; Petros *et al.*, 1992) and $^{12}C/^{12}C$-filtered COSY experiments (Ikura & Bax, 1992).

^1H, ^{15}N, ^{13}C, and ^{13}CO assignments and secondary structure determination of MMP-13 in the MMP-13:WAY-151693 complex were reported previously (Moy *et al.*, 2000). In addition to the NMR experiments used for the MMP-13 resonance assignments, the present structure is based on the following series of spectra: HNHA (Vuister & Bax, 1993), HNHB (Archer *et al.*, 1991), 3D long-range ^{13}C-^{13}C correlation (Bax & Pochapsky, 1992), coupled CT-HCACO (Powers *et al.*, 1991; Vuister *et al.*, 1992), HACAHB-COSY (Grzesiek *et al.*, 1995), 3D ^{15}N- (Marion *et al.*, 1989a; Zuiderweg & Fesik, 1989) and ^{13}C-edited NOESY (Ikura *et al.*, 1990; Zuiderweg *et al.*, 1990), and 3D ^{13}C-edited/^{12}C-filtered NOESY (Lee *et al.*, 1994) experiments. The ^{15}N-edited NOESY, ^{13}C-edited NOESY and 3D ^{13}C-edited/^{12}C-filtered NOESY experiments were collected with 100 ms, 120 ms and 110 ms mixing times, respectively. The acquisition parameters for each of the experiments used in determining the solution structure of MMP-13 complexed with WAY-151693 were as reported previously (Moy *et al.*, 1996).

The T_1 and T_2 data for the MMP-13:WAY-151693 complex were collected with 48 transients per increment. The T_1 inversion recovery times were T_1/20, 80, 140, 300, 500, 800 and 1200 ms, and the T_2 Carr-Purcell-Meiboom-Gill (CPMG) (Meiboom & Gill, 1958) trains were T_2/8, 24, 40, 72, 104 and 153 ms in duration (Kay *et al.*, 1992; Markley *et al.*, 1971). Recycle delays for T_1 and T_2 experiments were 1.7 and 1.3 seconds, respectively. Since the NOE measurement requires an equilibrated ^{15}N magnetization for accurate analysis, the recycle time was extended to more than six seconds while collecting 48 transients per increment. In the NOE experiment with presaturation, the proton saturation period was three seconds. ^1H saturation was carried out with the use of 180 ° ^1H pulses applied every 5 ms.

Spectra were processed using the NMRPipe software package (Delaglio *et al.*, 1995) and analyzed with PIPP (Garrett *et al.*, 1991) on a Sun Sparc Workstation. When appropriate, data processing included a solvent filter, zero-padding data to a power of 2, linear predicting back one data point of indirectly acquired data to obtain zero phase corrections, linear prediction of additional points for the indirectly acquired dimensions to increase resolution. Linear prediction by the means of the mirror image technique was used only for constant-time experiments (Zhu & Bax, 1992). In all cases, data were processed with a skewed sine-bell apodization function and one zero-filling was used in all dimensions.

NMR dynamics analysis

Peak heights were automatically assigned for each residue in all 2D spectra after semi-automatically peak picking one 2D spectra using NMRPipe. T_1 and T_2 values were determined by fitting the measured peak heights to the two-parameter profile $I(t) = I_o \exp(-t/T_n)$. The Levenberg-Maquardt algorithm (Press *et al.*, 1986) was used to determine the optimum values of T_n by minimizing the goodness of fit parameter, $\chi^2 = \Sigma\ (I_c(t) - I_e(t))^2/\sigma$, where $I_c(t)$ are the intensities calculated from the fitting parameters, $I_e(t)$ are the experimental intensities and σ is the standard deviation of the experimental intensities. Standard deviation (σ) was set to the rms baseline noise in the spectra as determined from NMRDraw. Uncertainty in T_1 and T_2 measurements were obtained from the covariance matrix generated in the Levenberg-Maquardt algorithm and were used in Monte Carlo simulation for determining the standard deviations for fitting parameters (Farrow *et al.*, 1994; Kamath & Shriver, 1989; Palmer *et al.*, 1991).

The steady-state NOE values were determined from the ratios of the intensities of the peaks with and without proton saturation. The standard deviation of the NOE value was determined by the baseline noise (Farrow *et al.*, 1994). The overall correlation time was determined by using residues that had ^{15}N T_1/T_2 ratios within one standard deviation and NOE values of greater than 0.6 (Clore *et al.*, 1990b; Clubb *et al.*, 1995; Kay *et al.*, 1989). Three models of the spectral density functions was used to classify five classes of optimized parameters (Clore *et al.*, 1990b,c; Farrow *et al.*, 1994; Kay *et al.*, 1989). Selection of the appropriate spectral density function was determined by initially fitting the data to the simplest spectral density function and selecting a more complicated spectral density function only as required to fit the data (Clore *et al.*, 1990b; Clubb *et al.*, 1995; Powers *et al.*, 1992).

Interproton distance restraints

The NOEs assigned from 3D ^{13}C-edited/^{12}C-filtered NOESY and 3D ^{15}N-edited NOESY experiments were classified into strong, medium, and weak corresponding to interproton distance restraints of 1.8-2.7 Å (1.8-2.9 Å for NOEs involving NH protons), 1.8-3.3 Å (1.8-3.5 Å for NOEs involving NH protons), and 1.8-5.0 Å , respectively (Clore *et al.*, 1986; Williamson *et al.*, 1985). Upper distance limits for distances involving methyl protons and non-stereospecifically assigned methylene protons were corrected appropriately for center averaging (Wuthrich *et al.*, 1983).

Torsion angle restraints and stereospecific assignments

The β-methylene stereospecific assignments and χ_1 torsion angle restraints were obtained primarily from a qualitative estimate of the magnitude of $^3J_{\alpha\beta}$ coupling constants from the HACAHB-COSY experiment (Grzesiek *et al.*, 1995) and $^3J_{N\beta}$ coupling constants from

the HNHB experiment (Archer *et al*., 1991). Further support for the assignments was obtained from approximate distance restraints for intraresidue NOEs involving NH, $C^{\alpha}H$, and $C^{\beta}H$ protons (Powers *et al*., 1993).

The ϕ and ψ torsion angle restraints were obtained from $^{3}J_{NH\alpha}$ coupling constants measured from the relative intensity of H^{α} crosspeaks to the NH diagonal in the HNHA experiment (Vuister & Bax, 1993), from a qualitative estimate of the magnitude of $^{3}J_{\alpha\beta}$ coupling constants from the HACAHB-COSY experiment (Grzesiek *et al*., 1995) and from approximate distance restraints for intraresidue and sequential NOEs involving NH, $C^{\alpha}H$, and $C^{\beta}H$ protons by means of the conformational grid search program STEREOSEARCH (Nilges *et al*., 1990) as described (Kraulis *et al*., 1989). $^{1}J_{C\alpha H\alpha}$ coupling constants obtained from a coupled 3D CT-HCACO spectrum were used to ascertain the presence of non-glycine residues with positive ϕ backbone torsion angles (Vuister *et al*., 1992). The presence of a $^{1}J_{C\alpha H\alpha}$ coupling constant greater then 130 Hz allowed for a minimum ϕ restraint of -2° to -178°.

The Ile and Leu χ_2 torsion angle restraints and the stereospecific assignments for leucine methyl groups were determined from $^{3}J_{C\alpha C\delta}$ coupling constants obtained from the relative intensity of C^{α} and C^{δ} crosspeaks in a 3D long-range ^{13}C-^{13}C NMR correlation spectrum (Bax *et al*., 1992), in conjunction with the relative intensities of intraresidue NOEs (Powers *et al*., 1993). Stereospecific assignments for valine methyl groups were determined based on the relative intensity of intraresidue NH-$C^{\gamma}H$ and $C^{\alpha}H$-$C^{\gamma}H$ NOEs as described (Zuiderweg *et al*., 1985). The minimum ranges employed for the ϕ, ψ, and χ torsion angle restraints were $\pm 30^{\circ}$, $\pm 50^{\circ}$, and $\pm 20^{o}$, respectively (Kraulis *et al*., 1989).

Structure calculations

The structures were calculated using the hybrid distance geometry-dynamical simulated annealing method of Nilges *et al*. (1988c) with minor modifications (Clore *et al*., 1990a) using the program X-PLOR (Brunger, 1993), adapted to incorporate pseudopotentials for $^{3}J_{NH\alpha}$ coupling constants (Garrett *et al*., 1994), secondary $^{13}C^{\alpha}/^{13}C^{\beta}$ chemical shift restraints (Kuszewski *et al*., 1995) and a conformational database potential (Kuszewski *et al*., 1996, 1997). The target function that is minimized during restrained minimization and simulated annealing comprises only quadratic harmonic terms for covalent geometry, $^{3}J_{NH\alpha}$ coupling constants and secondary $^{13}C^{\alpha}/^{13}C^{\beta}$ chemical shift restraints, square-well quadratic potentials for the experimental distance and torsion angle restraints, and a quartic van der Waals term for nonbonded contacts. All peptide bonds were constrained to be planar and *trans*. There was no hydrogen-bonding, electrostatic, or 6-12 Lennard-Jones empirical potential energy term in the target function.

To prevent the Zn and Ca ions from being expelled during the high-temperature simulated annealing stages of the refinement protocol, a minimal number of distance restraints between the His side-chain and Zn and between backbone atoms and Ca were included in the X-PLOR distance restraint file based on the observed coordination in the X-ray structures (Borkakoti *et al*., 1994; Lovejoy *et al*., 1994b,c; Spurlino *et al*., 1994).

The starting MMP-13:WAY-151693 complex structure for the simulated-annealing protocol was obtained by manually docking WAY-151693 into a homology model for MMP-13. The initial orientation of WAY-151693 in the MMP-13 active-site was based on the previously reported MMP-1:CGS-27023A structure (Moy *et al*., 1999). Given the general similarity in the overall fold for members of the MMP family, the use of a homology model for MMP-13 as a starting point for the structure refinement protocol was beneficial in expediting the iterative NOE analysis. A critical component for the analysis of ambiguous NOEs is the use of a distance filter based on the current structure during the structure refinement procedure. The value of the homology model for MMP-13 was to provide an initial distance filter for the analysis of ambiguous NOEs. Additionally, during the early stages of the structure refinement process with a minimal number of unambiguous NOE assignments, the structure conversion rate is typically very low, $\leqslant 30\,\%$. The utilization of the MMP-13 homology model increased the conversion rate to $\geqslant 70\,\%$, significantly improving the iterative process of analysis of ambiguous NOEs. The use of a homology model as a starting point for the analysis of ambiguous NOEs requires significant care to avoid biasing the final structure. This is achieved by applying a weighted preference in the decision-making process to data (unambiguous NOEs, dihedral constraints, etc.) that is not dependent on the homology model for obtaining the proper assignment.

Homology modeling

Homology modeling methods were utilized to generate a 3D model of MMP-13. The linear amino acid sequence corresponding to the catalytic domain of MMP-13 was aligned (SYBYL) with the catalytic domains of MMP-1, MMP-7 and MMP-8 based on the availability of their X-ray crystallographic structures (Betz *et al*., 1997; Bode *et al*., 1994; Borkakoti *et al*., 1994; Browner *et al*., 1995; Lovejoy *et al*., 1999; Spurlino *et al*., 1994). The alignments of MMP-13 with MMP-1 and MMP-8 demonstrated the highest homology where the computed identities are 58.9 % and 61.4 %, respectively.

The X-ray structure of MMP-8 was used as the template for homology modeling the structure of MMP-13. This decision was based mainly on the sequence alignment where no insertion is found in the critical specificity loop. In the specificity loop there is an ''insertion'' of two additional amino acid residues compared to the sequence length of MMP-1. Based on our analysis of the alignments, MMP-8 would allow for a more accurate modeling of the inhibitor binding pockets, since no prediction has to be made within this loop region.

COMPOSER (SYBYL) was used to construct the initial homology model of MMP-13. The only insertion was serine at position 29 of MMP-13. The insertion of S29 occurs within a coiled region that is at the entrance of a long α-helix and about 17 Å from the S′ specificity loop. The model of MMP-13 was then energy minimized utilizing a set of nested refinement procedures (Chen *et al*., 1993), but where the protein backbone heavy atoms were constrained as close to their original positions as possible.

The MMP-13:WAY-151693 model was then subjected to a 1000 steps of CHARMM minimization with the five intramolecular NOE restraints and the 47 distance restraints observed between MMP-13 and WAY-151693 where the coordinates for MMP-13 were kept fixed. This approach approximated the positioning of WAY-151693 in the active-site of MMP-13 without distorting the MMP-13 structure. The final structure was exported as a PDB file and used as the starting point for X-PLOR simulated annealing protocol where all the residues in

the structure were free to move. Since the initial stage of the simulated annealing protocol corresponds to high-temperature dynamics (1500 K) with a relatively weak X-PLOR NOE force constant (2), the initial MMP-13:WAY-151693 structure does not bias the structure determination process, since the structure is effectively free to explore the available conformational space. Additionally, each iteration of the simulated annealing process begins with a random trajectory for the molecular dynamics. That fact that these trajectories differ by upwards of 10 Å assures a distinct exploration of conformational space for the ensemble of MMP-13:WAY-151693 structures determined from the simulated annealing protocol.

Supplementary material

Tables of the resonance assignments, intra- and intermolecular NOEs for WAY-151693 in the MMP-13 complex are available from the authors upon request.

Protein Data Bank accession codes

Atomic coordinates for the 30 final simulated annealing structures and the restrained minimized mean structure of MMP-13 complexed with WAY-151693 have been deposited in the RCSB Protein Data Bank under accession PDB ID codes 1FM1 and 1FLS.

References

Archer, S. J., Ikura, M., Torchia, D. A. & Bax, A. (1991). An alternative 3D NMR technique for correlating backbone nitrogen-15 with side-chain H^{β} resonances in larger proteins. *J. Magn. Reson.* **95**, 636-641.

Balbin, M., Pendas, A. M., Uria, J. A., Jimenez, M. G., Freije, J. P. & Lopez-Otin, C. (1999). Expression and regulation of collagenase-3 (MMP-13) in human malignant tumors. *Apmis,* **107**, 45-53.

Bax, A. & Pochapsky, S. S. (1992). Optimized recording of heteronuclear multidimensional NMR spectra using pulsed field gradients. *J. Magn. Res.* **99**, 638-643.

Bax, A., Max, D. & Zax, D. (1992). Measurement of long-range ^{13}C-^{13}C *J* couplings in a 20-kDa protein-peptide complex. *J. Am. Chem. Soc.* **114**, 6923-6925.

Becker, J. W., Marcy, A. I. & Rokosz, L. L. (1995). Stromelysin-1: three-dimensional structure of the inhibited catalytic domain and of the C-truncated proenzyme. *Protein Sci.* **4**, 1966-1976.

Betz, M., Huxley, P., Davies, S. J., Mushtaq, Y., Pieper, M., Tschesche, H., Bode, W. & Gomis-Rueth, F. X. (1997). 1.8 Å crystal structure of the catalytic domain of human neutrophil collagenase (matrix metalloproteinase-8) complexed with a peptidomimetic hydroxamate primed-side inhibitor with a distinct selectivity profile. *Eur. J. Biochem.* **247**, 356-363.

Birkedal-Hansen, H., Moore, W. G. I., Bodden, M. K., Windsor, L. J., Birkedal-Hansen, B., DeCarlo, A. & Engler, J. A. (1993). Matrix metalloproteinases: a review. *Crit. Rev. Oral Biol. Med.* **4**, 197-250.

Bode, W., Reinemer, P., Huber, R., Kleine, T., Schnierer, S. & Tschesche, H. (1994). The X-ray crystal structure of the catalytic domain of human neutrophil collagenase inhibited by a substrate analog reveals the essentials for catalysis and specificity. *EMBO J.* **13**, 1263-1269.

Borkakoti, N., Winkler, F. K., Williams, D. H., D'Arcy, A., Broadhurst, M. J., Brown, P. A., Johnson, W. H. & Murray, E. J. (1994). Structure of the catalytic domain of human fibroblast collagenase complexed with an inhibitor. *Nature Struct. Biol.* **1**, 106-110.

Botos, I., Scapozza, L., Zhang, D., Liotta, L. A. & Meyer, E. F. (1996). Batimastat, a potent matrix metalloproteinase inhibitor, exhibits an unexpected mode of binding. *Proc. Natl Acad. Sci. USA,* **93**, 2749-2754.

Brooks, B. R., Bruccoleri, R. E., Olafson, B. D., States, D. J., Swaminathan, S. & Karplus, M. (1983). CHARMM: a program for macromolecular energy, minimization, and dynamics calculations. *J. Comput. Chem.* **4**, 187-217.

Broutin, I., Arnoux, B., Riche, C., Lecroisey, A., Keil, B., Pascard, C. & Ducruix, A. (1996). 1.8 Å structure of *Hypoderma lineatum* collagenase: a member of the serine proteinase family. *Acta Crystallog. sect. D,* **52**, 380-392.

Browner, M. F. (1995). Matrix metalloproteases: structure-based drug discovery targets. *Perspect. Drug Disc. Des.* **2**, 343-351.

Browner, M. F., Smith, W. W. & Castelhano, A. L. (1995). Crystal structures of matrilysin-inhibitor complexes. *Biochemistry,* **34**, 6602-6610.

Brunger, A. T. (1993). *X-PLOR Version 3.1 Manual*, Yale University, New Haven, CT.

Cawston, T. E. (1996). Metalloproteinase inhibitors and the prevention of connective tissue breakdown. *Pharmacol. Ther.* **70**, 163-182.

Chen, J. M., Sheldon, A. & Pincus, M. R. (1993). Structure-function correlations of calcium binding and calcium channel activities based on 3-dimensional models of human annexins I, II, III, V and VII. *J. Biomol. Struct. Dynam.* **10**, 1067-1089.

Clore, G. M. & Gronenborn, A. M. (1989). Determination of three-dimensional structures of proteins and nucleic acids in solution by nuclear magnetic resonance spectroscopy. *Crit. Rev. Biochem. Mol. Biol.* **24**, 479-564.

Clore, G. M., Nilges, M., Sukumaran, D. K., Bruenger, A. T., Karplus, M. & Gronenborn, A. M. (1986). The three-dimensional structure of α1-purothionin in solution: combined use of nuclear magnetic resonance, distance geometry and restrained molecular dynamics. *EMBO J.* **5**, 2729-2735.

Clore, G. M., Appella, E., Yamada, M., Matsushima, K. & Gronenborn, A. M. (1990a). Three-dimensional structure of interleukin 8 in solution. *Biochemistry,* **29**, 1689-1696.

Clore, G. M., Driscoll, P. C., Wingfield, P. T. & Gronenborn, A. M. (1990b). Analysis of the backbone dynamics of interleukin-1β using two-dimensional inverse detected heteronuclear nitrogen-15-proton NMR spectroscopy. *Biochemistry,* **29**, 7387-7401.

Clore, G. M., Szabo, A., Bax, A., Kay, L. E., Driscoll, P. C. & Gronenborn, A. M. (1990c). Deviations from the simple two-parameter model-free approach to the interpretation of nitrogen-15 nuclear magnetic relaxation of proteins. *J. Am. Chem. Soc.* **112**, 4989-4991.

Clubb, R. T., Omichinski, J. G., Sakaguchi, K., Appella, E., Gronenborn, A. M. & Clore, G. M. (1995). Backbone dynamics of the oligomerization domain of p53 determined from ^{15}N NMR relaxation measurements. *Protein Sci.* **4**, 855-862.

De, B., Natchus, M. G., Cheng, M., Pikul, S., Almstead, N. G., Taiwo, Y. O., Snider, C. E., Chen, L., Barnett,

B., Gu, F. & Dowty, M. (1999). The next generation of MMP inhibitors: design and synthesis. *Ann. NY Acad. Sci.* **878**, 40-60.

Delaglio, F., Grzesiek, S., Vuister, G. W., Zhu, G., Pfeifer, J. & Bax, A. (1995). NMRPipe: a multidimensional spectral processing system based on UNIX pipes. *J. Biomol. NMR,* **6**, 277-293.

Drummond, A. H., Beckett, P., Brown, P. D., Bone, E. A., Davidson, A. H., Galloway, W. A., Gearing, A. J. H., Huxley, P., Laber, D., McCourt, M., Whittaker, M., Wood, L. M. & Wright, A. (1999). Preclinical and clinical studies of MMP inhibitors in cancer. *Ann. NY Acad. Sci.* **878**, 228-235.

Farrow, N. A., Muhandiram, R., Singer, A. U., Pascal, S. M., Kay, C. M., Gish, G., Shoelson, S. E., Pawson, T., Forman-Kay, J. D. & Kay, L. E. (1994). Backbone dynamics of a free and a phosphopeptide-complexed Src homology 2 domain studied by ^{15}N NMR relaxation. *Biochemistry,* **33**, 5984-6003.

Freije, J. M. P., Diez-Itza, I., Balbin, M., Sanchez, L. M., Blasco, R., Tolivia, J. & Lopez-Otin, C. (1994). Molecular cloning and expression of collagenase-3 , a novel human matrix metalloproteinase produced by breast carcinomas. *J. Biol. Chem.* **269**, 16766-16773.

Garrett, D. S., Powers, R., Gronenborn, A. M. & Clore, G. M. (1991). A common sense approach to peak picking in two-, three-, and four-dimensional spectra using automatic computer analysis of contour diagrams. *J. Magn. Reson.* **95**, 214-220.

Garrett, D. S., Kuszewski, J., Hancock, T. J., Lodi, P. J., Vuister, G. W., Gronenborn, A. M. & Clore, G. M. (1994). The impact of direct refinement against three-bond HN-$C^{\alpha}H$ coupling constants on protein structure determination by NMR. *J. Magn. Reson. ser. B,* **104**, 99-103.

Gemmecker, G., Olejniczak, E. T. & Fesik, S. W. (1992). An improved method for selectivity observing protons attached to carbon-12 in the presence of proton-carbon-13 spin pairs. *J. Magn. Reson.* **96**, 199-204.

Ghose, A. K., Logan, M. E., Treasurywala, A. M., Wang, H., Wahl, R. C., Tomczuk, B. E., Gowravaram, M. R., Jaeger, E. P. & Wendoloski, J. J. (1995). Determination of pharmacophoric geometry for collagenase inhibitors using a novel computational method and its verification using molecular dynamics, NMR and X-ray crystallography. *J. Am. Chem. Soc.* **117**, 4671-4682.

Gonnella, N. C., Bohacek, R., Zhang, X., Kolossvary, I., Paris, C. G., Melton, R., Winter, C., Hu, S.-I. & Ganu, V. (1995). Bioactive conformation of stromelysin inhibitors determined by transferred nuclear Overhauser effects. *Proc. Natl Acad. Sci. USA,* **92**, 462-466.

Gonnella, N. C., Li, Y.-C., Zhang, X. & Paris, C. G. (1997). Bioactive conformation of a potent stromelysin inhibitor determined by X-nucleus filtered and multidimensional NMR spectroscopy. *Bioorg. Med. Chem.* **5**, 2193-2201.

Gooley, P. R., O'Connell, J. F. & Marcy, A. I. (1994). The NMR structure of the inhibited catalytic domain of human stromelysin-1. *Nature Struct. Biol.* **1**, 111-118.

Gooley, P. R., O'Connell, J. F., Marcy, A. I., Cuca, G. C., Axel, M. G., Caldwell, C. G., Hagmann, W. K. & Becker, J. W. (1996). Comparison of the structure of human recombinant short form stromelysin by multidimensional heteronuclear NMR and X-ray crystallography. *J. Biomol. NMR,* **7**, 8-28.

Grzesiek, S. & Bax, A. (1993). The importance of not saturating water in protein NMR. Application to sensitivity enhancement and NOE measurements. *J. Am. Chem. Soc.* **115**, 12593-12594.

Grzesiek, S., Kuboniwa, H., Hinck, A. P. & Bax, A. (1995). Multiple-quantum line narrowing for measurement of H.alpha.-H.beta. *J* couplings in isotopically enriched proteins. *J. Am. Chem. Soc.* **117**, 5312-5315.

Hajduk, P. J., Sheppard, G., Nettesheim, D. G. & Olejniczak, E. (1997). Discovery of potent nonpeptide inhibitors of stromelysin using SAR by NMR. *J. Am. Chem. Soc.* **119**, 5818-5827.

Ikura, M. & Bax, A. (1992). Isotope-filtered 2D NMR of a protein-peptide complex: study of a skeletal muscle myosin light chain kinase fragment bound to calmodulin. *J. Am. Chem. Soc.* **114**, 2433-2440.

Ikura, M., Kay, L. E., Tschudin, R. & Bax, A. (1990). Three-dimensional NOESY-HMQC spectroscopy of a carbon-13-labeled protein. *J. Magn. Reson.* **86**, 204-209.

Kamath, U. & Shriver, J. W. (1989). Characterization of thermotropic state changes in myosin subfragment-1 and heavy meromyosin by UV difference spectroscopy. *J. Biol. Chem.* **264**, 5586-5592.

Kay, L. E., Torchia, D. A. & Bax, A. (1989). Backbone dynamics of proteins as studied by nitrogen-15 inverse detected heteronuclear NMR spectroscopy: application to staphylococcal nuclease. *Biochemistry,* **28**, 8972-8979.

Kay, L. E., Nicholson, L. K., Delaglio, F., Bax, A. & Torchia, D. A. (1992). Pulse sequences for removal of the effects of cross correlation between dipolar and chemical-shift anisotropy relaxation mechanisms on the measurement of heteronuclear T1 and T2 values in proteins. *J. Magn. Reson.* **97**, 359-375.

Kraulis, P. J., Clore, G. M., Nilges, M., Jones, T. A., Pettersson, G., Knowles, J. & Gronenborn, A. M. (1989). Determination of the three-dimensional solution structure of the C-terminal domain of cellobiohydrolase I from *Trichoderma reesei*. A study using nuclear magnetic resonance and hybrid distance geometry-dynamical simulated annealing. *Biochemistry,* **28**, 7241-7257.

Kuszewski, J., Qin, J., Gronenborn, A. M. & Clore, G. M. (1995). The impact of direct refinement against $^{13}C^{\alpha}$ and $^{13}C^{\beta}$ chemical shifts on protein structure determination by NMR. *J. Magn. Reson. ser. B,* **106**, 92-96.

Kuszewski, J., Gronenborn, A. M. & Clore, G. M. (1996). Improving the quality of NMR and crystallographic protein structures by means of a conformational database potential derived from structure databases. *Protein Sci.* **5**, 1067-1080.

Kuszewski, J., Gronenborn, A. M. & Clore, G. M. (1997). Improvements and extensions in the conformational database potential for the refinement of NMR and X-ray structures of proteins and nucleic acids. *J. Magn. Reson.* **125**, 171-177.

Laskowski, R. A., MacArthur, M. W., Moss, D. S. & Thornton, J. M. (1993). PROCHECK: a program to check the stereochemical quality of protein structures. *J. Appl. Crystallog.* **26**, 283-291.

Lee, W., Revington, M. J., Arrowsmith, C. & Kay, L. E. (1994). A pulsed field gradient isotope-filtered 3D ^{13}C HMQC-NOESY experiment for extracting intermolecular NOE contacts in molecular complexes. *FEBS Letters,* **350**, 87-90.

Lovejoy, B., Cleasby, A. & Hassell, A. M. (1994a). Structural analysis of the catalytic domain of human

fibroblast collagenase. *Ann. NY Acad. Sci.* **732**, 375-378.

Lovejoy, B., Cleasby, A. & Hassell, A. M. (1994b). Structure of the catalytic domain of fibroblast collagenase complexed with an inhibitor. *Science,* **263**, 375-377.

Lovejoy, B., Hassell, A. M. & Luther, M. A. (1994c). Crystal structures of recombinant 19-kDa human fibroblast collagenase complexed to itself. *Biochemistry,* **33**, 8207-8217.

Lovejoy, B., Welch, A. R., Carr, S., Luong, C., Broka, C., Hendricks, R. T., Campbell, J. A., Walker, K. A. M., Martin, R., Van Wart, H. & Browner, M. F. (1999). Crystal structures of MMP-1 and -13 reveal the structural basis for selectivity of collagenase inhibitors. *Nature Struct. Biol.* **6**, 217-221.

Marion, D., Driscoll, P. C., Kay, L. E., Wingfield, P. T., Bax, A., Gronenborn, A. M. & Clore, G. M. (1989a). Overcoming the overlap problem in the assignment of proton NMR spectra of larger proteins by use of three-dimensional heteronuclear proton-nitrogen-15 Hartmann-Hahn-multiple quantum coherence and nuclear Overhauser-multiple quantum coherence spectroscopy: application to interleukin 1. beta. *Biochemistry,* **28**, 6150-6156.

Marion, D., Ikura, M., Tschudin, R. & Bax, A. (1989b). Rapid recording of 2D NMR spectra without phase cycling: application to the study of hydrogen exchange in proteins. *J. Magn. Reson.* **85**, 393-399.

Markley, J. L., Horsley, W. J. & Klein, M. P. (1971). Spin-lattice relaxation measurements in slowly relaxing complex spectra. *J. Chem. Phys.* **55**, 3604-3605.

Meiboom, S. & Gill, D. (1958). Modified spin-echo method for measuring nuclear relaxation times. *Rev. Sci. Instrum.* **29**, 688-691.

Morphy, J. R., Millican, T. A. & Porter, J. R. (1995). Matrix metalloproteinase inhibitors: current status. *Curr. Med. Chem.* **2**, 743-762.

Moy, F. J., Seddon, A. P., Boehlen, P. & Powers, R. (1996). High-resolution solution structure of basic fibroblast growth factor determined by multidimensional heteronuclear magnetic resonance spectroscopy. *Biochemistry,* **35**, 13552-13561.

Moy, F. J., Pisano, M. R., Chanda, P. K., Urbano, C., Killar, L. M., Sung, M.-L. & Powers, R. (1997). Assignments, secondary structure and dynamics of the inhibitor-free catalytic fragment of human fibroblast collagenase. *J. Biomol. NMR,* **10**, 9-19.

Moy, F. J., Chanda, P. K., Cosmi, S., Pisano, M. R., Urbano, C., Wilhelm, J. & Powers, R. (1998). High-resolution solution structure of the inhibitor-free catalytic fragment of human fibroblast collagenase determined by multidimensional NMR. *Biochemistry,* **37**, 1495-1504.

Moy, F. J., Chanda, P. K., Chen, J. M., Cosmi, S., Edris, W., Skotnicki, J. S., Wilhelm, J. & Powers, R. (1999). NMR solution structure of the catalytic fragment of human fibroblast collagenase complexed with a sulfonamide derivative of a hydroxamic acid compound. *Biochemistry,* **38**, 7085-7096.

Moy, F. J., Chanda, P. K., Cosmi, S., Edris, W., Levin, J. I. & Powers, R. (2000). ^{1}H, ^{15}N, ^{13}C, and ^{13}CO assignments and secondary structure determination of collagenase-3 (MMP-13) complexed with a hydroxamic acid inhibitor. *J. Biomol. NMR,* **17**, 269-270.

Netzel-Arnett, S., Sang, Q. X., Moore, W. G. I., Navre, M., Birkedal-Hansen, H. & Van Wart, H. E. (1993). Comparative sequence specificities of human 72- and 92-kDa gelatinases (type IV collagenases) and PUMP (matrilysin). *Biochemistry,* **32**, 6427-6432.

Nilges, M., Clore, G. M. & Gronenborn, A. M. (1988a). Determination of three-dimensional structures of proteins from interproton distance data by dynamical simulated annealing from a random array of atoms. Circumventing problems associated with folding. *FEBS Letters,* **239**, 129-136.

Nilges, M., Clore, G. M. & Gronenborn, A. M. (1988b). Determination of three-dimensional structures of proteins from interproton distance data by hybrid distance geometry-dynamical stimulated annealing calculations. *FEBS Letters,* **229**, 317-324.

Nilges, M., Gronenborn, A. M., Bruenger, A. T. & Clore, G. M. (1988c). Determination of three-dimensional structures of proteins by simulated annealing with interproton distance restraints. Application to crambin, potato carboxypeptidase inhibitor and barley serine proteinase inhibitor 2. *Protein Eng.* **2**, 27-38.

Nilges, M., Clore, G. M. & Gronenborn, A. M. (1990). Proton NMR stereospecific assignments by conformational data-base searches. *Biopolymers,* **29**, 813-822.

Olejniczak, E. T., Hajduk, P. J., Marcotte, P. A. & Nettesheim, D. G. (1997). Stromelysin inhibitors designed from weakly bound fragments: effects of linking and cooperativity. *J. Am. Chem. Soc.* **119**, 5828-5832.

Palmer, A. G., III, Rance, M. & Wright, P. E. (1991). Intramolecular motions of a zinc finger DNA-binding domain from Xfin characterized by proton-detected natural abundance carbon-13 heteronuclear NMR spectroscopy. *J. Am. Chem. Soc.* **113**, 4371-4380.

Petros, A. M., Kawai, M., Luly, J. R. & Fesik, S. W. (1992). Conformation of two non-immunosuppressive FK506 analogs when bound to FKBP by isotope-filtered NMR. *FEBS Letters,* **308**, 309-314.

Piotto, M., Saudek, V. & Sklenar, V. (1992). Gradient-tailored excitation for single-quantum NMR spectroscopy of aqueous solutions. *J. Biomol. NMR,* **2**, 661-665.

Powell, W. C. & Matrisian, L. M. (1996). Complex roles of matrix metalloproteinases in tumor progression. *Curr. Top. Microbiol. Immunol.* **213**, 1-21.

Powers, R., Gronenborn, A. M., Clore, G. M. & Bax, A. (1991). Three-dimensional triple-resonance NMR of carbon-13/nitrogen-15-enriched proteins using constant-time evolution. *J. Magn. Reson.* **94**, 209-213.

Powers, R., Clore, G. M., Stahl, S. J., Wingfield, P. T. & Gronenborn, A. (1992). Analysis of the backbone dynamics of the ribonuclease H domain of the human immunodeficiency virus reverse transcriptase using nitrogen-15 relaxation measurements. *Biochemistry,* **31**, 9150-9157.

Powers, R., Garrett, D. S., March, C. J., Frieden, E. A., Gronenborn, A. M. & Clore, G. M. (1993). The high-resolution, three-dimensional solution structure of human interleukin-4 determined by multidimensional heteronuclear magnetic resonance spectroscopy. *Biochemistry,* **32**, 6744-6762.

Press, W. M., Flannery, B. P., Teukolsky, S. A. & Vetterling, W. T. (1986). *Numerical Recipes*, Cambridge University Press, Cambridge, UK.

Ries, C. & Petrides, E. (1995). Cytokine regulation of matrix metalloproteinase activity and its regulatory dysfunction in disease. *Biol. Chem. Hoppe-Seyler,* **376**, 345-355.

Rockwell, A., Melden, M., Copeland, R. A., Hardman, K., Decicco, C. P. & DeGrado, W. F. (1996). Complementarity of combinatorial chemistry and structure-based ligand design: application to the discovery of novel inhibitors of matrix metalloproteinases. *J. Am. Chem. Soc.* **118**, 10337-10338.

Spera, S. & Bax, A. (1991). Empirical correlation between protein backbone conformation and C^{α} and C^{β} ^{13}C nuclear magnetic resonance chemical shifts. *J. Am. Chem. Soc.* **113**, 5490-5492.

Spurlino, J. C., Smallwood, A. M., Carlton, D. D., Banks, T. M., Vavra, K. J., Johnson, J. S., Cook, E. R., Falvo, J. & Wahl, R. C., *et al*. (1994). 1.56 Å structure of mature truncated human fibroblast collagenase. *Proteins: Struct. Funct. Genet.* **19**, 98-109.

Stams, T., Spurlino, J. C., Smith, D. L., Wahl, R. C., Ho, T. F., Qoronfleh, M. W., Banks, T. M. & Rubin, B. (1994). Structure of human neutrophil collagenase reveals large S1′ specificity pocket. *Nature Struct. Biol.* **1**, 119-123.

Van Doren, S. R., Kurochkin, A. V., Hu, W., Ye, Q.-Z., Johnson, L. L., Hupe, D. J. & Zuiderweg, E. R. P. (1995). Solution structure of the catalytic domain of human stromelysin complexed with a hydrophobic inhibitor. *Protein Sci.* **4**, 2487-2498.

Vuister, G. W. & Bax, A. (1993). Quantitative *J* correlation: a new approach for measuring homonuclear three-bond *J*(HNHα) coupling constants in ^{15}N-enriched proteins. *J. Am. Chem. Soc.* **115**, 7772-7777.

Vuister, G. W., Delaglio, F. & Bax, A. (1992). An empirical correlation between $^{1}J_{C\alpha H\alpha}$ and protein backbone conformation. *J. Am. Chem. Soc.* **114**, 9674-9675.

Williamson, M. P., Havel, T. F. & Wuthrich, K. (1985). Solution conformation of proteinase inhibitor IIA from bull seminal plasma by proton nuclear magnetic resonance and distance geometry. *J. Mol. Biol.* **182**, 295-315.

Woessner, J. F., Jr (1991). Matrix metalloproteinases and their inhibitors in connective tissue remodeling. *FASEB J.* **5**, 2145-2154.

Wuthrich, K., Billeter, M. & Braun, W. (1983). Pseudo-structures for the 20 common amino acids for use in studies of protein conformation by measurements of intramolecular proton-proton distance constraints with nuclear magnetic resonance. *J. Mol. Biol.* **169**, 949-961.

Zask, A., Levin, J. I., Killar, L. M. & Skotnicki, J. S. (1996). Inhibition of matrix metalloproteinases: structure based design. *Curr. Pharm. Des.* **2**, 624-661.

Zhu, G. & Bax, A. (1992). Improved linear prediction of damped NMR signals using modified ''forward-backward'' linear. *J. Magn. Reson.* **100**, 202-207.

Zuiderweg, E. R. P. & Fesik, S. W. (1989). Heteronuclear three-dimensional NMR spectroscopy of the inflammatory protein C5a. *Biochemistry,* **28**, 2387-2391.

Zuiderweg, E. R. P., Boelens, R. & Kaptein, R. (1985). Stereospecific assignments of proton-NMR methyl lines and conformation of valyl residues in the lac repressor headpiece. *Biopolymers,* **24**, 601-611.

Zuiderweg, E. R. P., McIntosh, L. P., Dahlquist, F. W. & Fesik, S. W. (1990). Three-dimensional carbon-13-resolved proton NOE spectroscopy of uniformly carbon-13-labeled proteins for the NMR assignment and structure determination of larger molecules. *J. Magn. Reson.* **86**, 210-216.

Edited by M. F. Summers

(Received 3 May 2000; received in revised form 31 July 2000; accepted 31 July 2000)